"Blind" Calibration and Toeplitz Covariance Matrix Estimation in Uniform Linear Arrays. Part I. Benchmark Analysis and Matrix-Free Techniques.

Yuri Abramovich, *Life Fellow, IEEE*, Tanit Pongsiri

***Abstract*-The problems of uniform linear array (with uniform mutual coupling) calibration and Toeplitz covariance matrix estimation are re-examined for application in the receive arrays of modern High Frequency Over-the-Horizon Radars (HF OTHR). Specifics of these arrays, operating predominantly in the "over-sampled" ($d/\lambda < 0.5$) regime, are exploited along with the recent findings in the Toeplitz Inverse Eigenvalue problem (ToIEP), Random Matrix Theory, and the "Expected Likelihood" methodology developed earlier to advance the problem solution. In this paper we re-evaluate the benchmark efficiency of the "blind" calibration and analyze several techniques that are based on certain properties of the Toeplitz covariance matrix and "over-sampled" uniform antenna arrays, but do not require matrix estimation. In Part II we analyze the case of the unknown symmetric and Hermitian Toeplitz matrices and introduce techniques for joint antenna calibration and Toeplitz covariance matrix estimation.**

***Index Terms*—Analysis of Toeplitzification routines**

I. Introduction

Most of the modern High Frequency Over-the-Horizon-Radars (HF OTHR), such as the Australian JORN [1] have a very long aperture (~3 km) for their uniform linear receive antenna arrays (ULA's) that have several hundred receive antenna elements. These arrays are usually located in remote areas and have an accurately engineered uniform near field. These arrays operate within the entire HF band (5 MHz-30 MHz), depending on ionospheric propagation conditions. This very accurate implementation of the antenna and its near field allow for an accurate enough description of these arrays by uniform mutual coupling. In order to avoid grating lobes, the inter-element spacing in these arrays is selected to match the $d/\lambda = 0.5$ condition at the higher end of the HF band above, say, f = 25 MHz. For this reason, most of time these arrays operate in the so-called "over-sampled" regime, with $d/\lambda < 0.5$. Naturally, the mutual coupling gets stronger in the "over-sampled" regime. And yet, the homogeneous ULA design allows for selection within the ~3 km aperture of a long enough "internal" ULA sub-array with all elements experiencing equal mutual coupling. Indeed, for a 3 km long aperture, the antenna "edges" extend over (2+3)λ (with inhomogeneous mutual coupling) and insignificantly reduces the "internal" array aperture dimension with homogeneous mutual coupling. For this reason, in this study we consider the truly uniform ULA, which is basically the central sub-array of the entire receive antenna array. Peripheral antenna elements in this regime are used as "dummy" elements, equalizing the mutual coupling of the active central antenna elements. Note that in some designs with a relatively short antenna aperture such as, for example, the Surface Wave HF OTHR [2], the properly loaded "dummy" antenna elements (with no receivers attached) are used to equalize the mutual coupling of the internal active antenna elements.

Of course, in order to calibrate the entire array aperture within the entire HF band, one has to consider the differences in the mutual coupling within the "edge" elements. Yet, in this paper we concentrate on operations with a truly uniform linear array with uniform (Toeplitz matrix) mutual coupling that allows for ignoring the presence of this coupling for the problems of interest. Operations on the entire array aperture with the non-homogeneous "edge" elements are analyzed in Part III of this series. Since operations on the uniform "internal" sub-array are an integral part of the entire array processing, the detailed analysis of the strictly uniform linear sub-array processing is of essential importance.

To support operations in active HF OTHR mode at a pre-selected operational frequency, certain instrumental means with the specific test signals are currently considered to calibrate this receive array prior to active illumination. Yet, the broad introduction of the so-called "Direct Digital Receivers" (DDRx), with analog-to-digital conversion (ADC) of the entire HF band [3], provides concurrent access to multiple receive channels operating within the entire HF band. The traditional techniques for active radar mode antenna calibration are inadequate for concurrent simultaneous array calibration for a large number of frequency channels across the entire HF band. Naturally, the attention is focused on the methods of the so-called "blind" antenna calibration that uses intercepted signals of interest within a given frequency channel.

It is important to mention that "blind" antenna calibration techniques for ULA's are one of the well-investigated problems by many authors, starting with the pioneering paper by A. Paulaj and T. Kailath in 1985 [4]. A very informative review of the numerous publications is introduced in [5], for example. And yet, despite the reach of publications and quite exhaustive results gained so far, we return to this problem mostly due to the specifics of the receive arrays of the HF OTHR operating in passive mode. The prime interest in this mode is the analysis of the non-cooperative HF OTHR activity. The most powerful intercepted signals are the clutter returns from the illuminated part of the Earth's surface. Obviously, these clutter returns

Yuri Abramovich and Tanit Pongsiri are with WR Systems, Ltd., Fairfax, VA 22030, USA. Emails: yabramovich@wrsystems.com, tpongsiri@wrsystems.com

differ significantly from a number of point sources, considered in applications, associated with the direction of arrival (DOA) estimation problem. Since HF OTHR receive (Rx) antenna arrays often operate in the oversampled regime ($d/\lambda < 0.5$), the clutter returns occupy only the visible sector, while the presence of "invisible" angles may be used for antenna calibration. In [6] we analyzed this possibility, but it has not been fully explored in [6]. Moreover, in many cases the beampattern of the transmit antenna of a non-cooperative HF OTHR is known to be a symmetric function (in $\mu = \sin\theta$ coordinates). Therefore, under favorable propagation conditions the a priori unknown covariance matrix may be treated as a symmetric (real-valued) Toeplitz matrix, linearly shifted into the illumination direction angle. This property of the covariance matrix (in the properly calibrated ULA) may also be used for efficient calibration. Yet, in the case of multi-mode propagation with an azimuthal shift, which is different for different propagation modes, the spatial covariance matrix received by a properly calibrated ULA will be an arbitrary Hermitian Toeplitz covariance matrix. Luckily, the "invisible" sector of the over-sampled ULA may still be used to assist the array calibration in this different scenario. Note, that in many practical applications, the spatial covariance matrix of the signals of interest needs to be estimated regardless of the array calibration problem. Therefore, the relative performance of the joint array calibration and spatial covariance matrix assessment, with respect to the antenna calibration techniques that do not require the covariance matrix estimates, is of practical interest for such applications.

Finally, many of the techniques developed so far reliably operate only when the calibration errors are small and the estimation phase wrapping problem does not exist. For example, in [5] the authors assumed that the phase offsets are relatively "small", i.e.

$$|\varphi_j| \ll x \quad \forall_i \in \{1, \dots, N\},$$

to avoid association with the phase wrapping problem. Obviously, it is important to overcome this limitation. One extra issue needs to be specified in this regard. Starting from the pioneering paper in [4], a common feature of the developed techniques was that the phase errors could be determined up to an arbitrary linear progressive phase shift across the array. This in turn means that "the best we can hope for to do is to find DOA's to within an arbitrary rotation factor" [4]. For our HF OTHR applications, this situation is not that hopeless. First, some of the introduced techniques are capable of a proper calibration despite being affected by the parasitic linear phase progression. Secondly, if the performed calibration is capable of non-linear and random-like phase errors removal but the removal is associated with a bias, then this bias may be removed using the ever present galactic point sources with precisely known coordinates, such as the radio star Cygnus-A, for example. These stellar sources are too weak for proper antenna calibration, but for bias removal in a properly calibrated ~3 km-long ULA array, they are powerful enough at the output of the beam steered in the stellar source direction. The problems described above define the content of this Part I paper.

First, after the problem formulation, we introduce the test on the Toeplitz nature of the original true matrix of the given sample matrix. In other words, this tests that a given sample matrix is created by a positive definite (p.d.) Toeplitz covariance matrix. This test should allow for detection of the calibration phase errors and checks the quality of the antenna calibration. At the same time, maximization of this test value should allow for direct "calibration" phase errors removal.

The second problem addressed in this paper is the re-evaluation of the benchmark efficiency provided by the Maximum Likelihood (ML) estimation algorithm for the scenario with the a priori known true covariance matrix of the signals at the output of the ideally calibrated array. The benchmark allows for the evaluation of the relative efficiency of other techniques analyzed in this paper. Specifically, this benchmark is used to evaluate the efficiency of the "invariant" techniques that do not require the true Toeplitz covariance matrix knowledge. This is the technique proposed by A. Paulaj and T. Kaileth in [4] and modified in [5]. This technique exploits the properties of the Toeplitz covariance matrix but do not require the matrix knowledge. The same benchmark technique is then used for efficiency evaluation of the "over-sampled" array calibration, where the existing "invisible" region is used for the array calibration.

Therefore, in Part I of this paper we investigate the benchmark ULA calibration performance and evaluate the relative performance merits of the "invariant" techniques that do not require covariance matrix estimation. In Part II of this series, we investigate the efficiency of the joint ULA array calibration and Toeplitz covariance matrix estimation, and compare the efficiency of this joint estimation technique with the benchmark and "invariant" techniques efficiency investigated in Part I. In Part III of this paper, we report on the efficiency of the entire ULA aperture calibration efficiency with respect to the inhomogeneous mutual coupling that affects the edge elements of the ULA of the HF OTHR.

II. Problem Formulation and the Test on the Structure of the Sample Matrix Origin

Let the *N*-element ULA receive the signals $\mathbf{Y}_t \in \mathbb{C}^{N\,x\,1}, t = 1, \dots, T$ that may be represented as:

$$\mathbf{Y}_t = \mathbf{D}(\mathbf{\Phi}_{N-1})\mathbf{T}_N^{\frac{1}{2}}\boldsymbol{\xi}_t, \quad \boldsymbol{\xi}_t \sim \mathbb{C}\mathcal{N}(0, \mathbf{I}_N), \quad t = 1, \dots, T \tag{1}$$

where

$$\mathbf{D}(\mathbf{\Phi}_{N-1}) = \mathrm{diag}[1, e^{i\boldsymbol{\varphi}_1}, \dots, e^{i\boldsymbol{\varphi}_{N-1}}], \tag{2}$$

where $\boldsymbol{\varphi}_l$ $(\boldsymbol{\varphi}_0 = 0^{\mathrm{o}}), l = 0, \dots, N-1$ are the calibration phase errors that may include the progressive linear trend:

$$\boldsymbol{\varphi}_l = \begin{cases} \boldsymbol{\varphi}_l^{\mathrm{o}} + \dfrac{2\pi d}{\lambda} l \sin\theta_0, & l = 0, \dots, N-1 \\ \text{or} \\ \boldsymbol{\varphi}_l^{\mathrm{o}} \end{cases} \tag{3}$$

where

$$-\boldsymbol{\varphi}_{max} < \boldsymbol{\varphi}_l \le \boldsymbol{\varphi}_{max}, \quad \text{with } \boldsymbol{\varphi}_{max} \le \pi\,. \tag{4}$$

In (1), $\mathbf{T}_N$ is the Toeplitz spatial covariance matrix of the signals impinging upon the array that are not affected by the phase "calibration" errors. As discussed in Introduction, in HF OTHR applications, the Rx antenna usually operates in the so-called "over-sampled" regime when

$$d/\lambda < 0.5, \tag{5}$$

where d is the inter-element spacing and λ is the wavelength. Correspondingly, the "visible" sector

$$0 \le |\mu| \le 2\pi d/\lambda \tag{6}$$

occupies only a part of the function $\mu = 2\pi d/\lambda \ \sin\theta$ while the rest of the period

$$2\pi d/\lambda \le |\mu| \le \pi \tag{7}$$

forms a sector of the so-called "invisible" angles.

The actual covariance matrix $\mathbf{T}_N$ of the signals, impinging upon a (calibrated) ULA, depends on the beamwidth of the transmitting (Tx) antenna array and on the propagation conditions, with a spectrum that always entirely resides within the visible region $|\sin\theta| < 1$. With respect to the calibration phase errors (3), the spatial covariance matrix is affected by the phase "calibration" errors of the antenna array and may be presented as

$$\mathbf{R}_N = \mathbf{D}[\boldsymbol{\Phi}_{N-1}]\mathbf{T}_N\mathbf{D}^{\mathrm{H}}[\boldsymbol{\Phi}_{N-1}] + \sigma_n^2\mathbf{I}_N\,, \tag{8}$$

where σ_n^2 is the power of the internal additive white noise. Depending on the problem, we may present the covariance matrix $\mathbf{R}_N$ as

$$\mathbf{R}_N = \mathbf{D}[\boldsymbol{\Phi}^{\mathbf{o}}_{\boldsymbol{N-1}}]\mathbf{T}_N\mathbf{D}^{\mathrm{H}}[\boldsymbol{\Phi}^{\mathbf{o}}_{\boldsymbol{N-1}}] + \sigma_n^2\mathbf{I}_N \tag{9}$$

where $\boldsymbol{\Phi}^{\mathbf{o}}_{\boldsymbol{N-1}}$ does not include the linear phase progression and $\mathbf{T}_N$ is a Hermitian Toeplitz covariance matrix, or in some cases as

$$\mathbf{R}_N = \mathbf{D}[\boldsymbol{\Phi}_{N-1}]\mathbf{T}^{\mathrm{S}}_N\mathbf{D}^{\mathrm{H}}[\boldsymbol{\Phi}_{N-1}] + \sigma_n^2\mathbf{I}_N, \tag{10}$$

where $\mathbf{T}^{\mathrm{S}}_N$ is a symmetric (real-valued) Toeplitz matrix and $\mathbf{D}[\boldsymbol{\Phi}_{N-1}]$ does includes the linear phase progression (3).

As discussed in Introduction, in some active HF OTHR modes, the angular spectrum of the illuminated area and therefore, the spatial covariance matrix $\mathbf{T}_N$ specified by the Tx antenna beampattern and propagation conditions, may be treated as known a priori (with a certain accuracy). In most passive mode operations the Toeplitz spatial covariance matrix is not known a priori. Yet, if the Tx beampattern is known to be symmetric (in $\mu = \sin\theta$ coordinates) then the spatial covariance matrix may be presented in the form (10) with the symmetric (real-valued) Toeplitz covariance matrix $\mathbf{T}_N$. In the properly calibrated "oversampled" ULA, no power in excess of the beampattern sidelobes "leaking" into the invisible region should be "seen" in the "invisible" sector (7).

For the analytical description of the operational ULA, let us now assume that for the given set of T independent identically distributed (i.i.d.) training samples $\mathbf{Y}_t, t = 1, \dots, T$ (1)-(4), we have to decide on whether these samples are "generated" in (1) by a Toeplitz or non-Toeplitz covariance matrix. We expect that this test should allow for detection of the "calibration" phase errors and evaluate the accuracy of the array calibration. In other words, we have to decide on whether the sample matrix $\widehat{\mathbf{R}}_N$

$$\widehat{\mathbf{R}}_N = \frac{1}{T}\sum_{t=1}^{T}\mathbf{Y}_t\mathbf{Y}_t^{\mathrm{H}}, \tag{11}$$

created by the samples $\mathbf{Y}_t \sim \mathbb{C}\mathcal{N}(0, \mathbf{T}_N)$, is generated by a $\mathbf{T}_N$ that is a p.d. Toeplitz Hermitian matrix or not. Note, that in order to check that the sample matrix $\widehat{\mathbf{R}}_N$ originates from the covariance matrix $c\mathbf{R}_N$, $c > 0$, one can use the "sphericity" likelihood ratio test (LR) [7],

$$\mathrm{LR}\big(\widehat{\mathbf{R}}_N\big|\mathbf{R}_N\big) = \frac{\det[\widehat{\mathbf{R}}_N\mathbf{R}_N^{-1}]}{[\frac{1}{N}\mathrm{Tr}[\widehat{\mathbf{R}}_N\mathbf{R}_N^{-1}]]^N} \underset{\mathrm{H}_0}{\overset{\mathrm{H}_1}{\gtrless}} \gamma_o\,. \tag{12}$$

The advantage of this test is the pdf of the $\mathrm{LR}\big(\widehat{\mathbf{R}}_N\big|\mathbf{R}_N\big)$ for the hypothesis H_1 ($\mathrm{E}\big[\widehat{\mathbf{R}}_N\big] = c\mathbf{R}_N$), does not depend on $\mathbf{R}_N$. Indeed, if

$$\widehat{\mathbf{R}}_N = \frac{c}{T}\sum_{t=1}^{T}\mathbf{R}_N^{1/2}\boldsymbol{\xi}_t\boldsymbol{\xi}_t^{\mathrm{H}}\mathbf{R}_N^{1/2}, \quad \boldsymbol{\xi}_t \sim \mathbb{C}\mathcal{N}(0, \mathbf{I}_N), c > 0 \tag{13}$$

then

$$\mathrm{LR}\big(\widehat{\mathbf{R}}_N\big|\mathbf{R}_N\big) = \frac{\det[\frac{1}{T}\sum_{t=1}^{T}\boldsymbol{\xi}_t\boldsymbol{\xi}_t^{\mathrm{H}}]}{[\frac{1}{NT}\mathrm{Tr}[\boldsymbol{\xi}_t\boldsymbol{\xi}_t^{\mathrm{H}}]]^N} \tag{14}$$

where $\boldsymbol{\xi}_t \sim \mathbb{C}\mathcal{N}(0, \mathbf{I}_N)$. Distribution of the LR test (14) is specified by (*N, T)* only and therefore, could be precalculated. The actual pdf for (14) is introduced in [8].

In our problem, the Toeplitz covariance matrix $\mathbf{T}_N$ is not known a priori and the idea for our approach is to use the p.d. Toeplitz Hermitian matrix "closest" to $\widehat{\mathbf{R}}_N$. The expectation is that if $\mathrm{E}\big[\widehat{\mathbf{R}}_N\big] = \mathbf{T}_N$, then the Toeplitz matrix "closest" to $\widehat{\mathbf{R}}_N$ should possess the invariance property similar to (17). Unfortunately, the closed form solution for the maximum likelihood (ML) Toeplitz matrix estimate, given the sample matrix $\widehat{\mathbf{R}}_N$ (11), does not exist. The well-known "Toeplitzisation" [9] or "redundancy averaging" [10], often used for transformation of the sample matrix $\widehat{\mathbf{R}}_N$ into a Toeplitz matrix, for most practical cases is inappropriate since it results in a "non-positive definite" Toeplitz matrix [10]. For this

reason, we use the suggested transformation in [11] of the p.d. sample matrix $\widehat{\mathbf{R}}_N$ into a p.d. Toeplitz Hermitian matrix $\mathbf{T}_N$ with the same maximum entropy spectrum, i.e.

$$\frac{\widehat{\mathbf{R}}_N^{-1}\boldsymbol{e}_1}{\mathbf{e}_1^{\mathrm{T}}\widehat{\mathbf{R}}_N^{-1}\boldsymbol{e}_1} = \frac{\widehat{\mathbf{T}}_N^{-1}\boldsymbol{e}_1}{\mathbf{e}_1^{\mathrm{T}}\widehat{\mathbf{T}}_N^{-1}\boldsymbol{e}_1}, \quad \mathbf{e}_1^{\mathrm{T}} = (1,0,\dots,0)\,. \tag{15}$$

According to the Lemma introduced in [11], in order for an arbitrary N-variate vector $\mathbf{P}$ with $p_1 > 0$ to be represented in the form

$$p = \widehat{\mathbf{T}}_N^{-1}\boldsymbol{e}_1 \tag{16}$$

where $\mathbf{T}_N$ is a p.d. Hermitian Toeplitz matrix, it is necessary and sufficient that the polynomial

$$\mathbf{P}(\mathrm{z}) = \sum_{n=1}^{N} \mathbf{P}_n\, \mathbf{z}^{n-1} \tag{17}$$

has no zeros inside the unit disk:

$$\mathbf{P}(\mathrm{z}) \neq 0, \ \text{ for } |z| < 1\,. \tag{18}$$

Given this Lemma, the problem of p.d. Toeplitz matrix reconstruction given the sample vector $\widehat{\mathbf{W}}$, where

$$\widehat{\mathbf{W}} = \frac{\widehat{\mathbf{R}}_N^{-1}\boldsymbol{e}_1}{\mathbf{e}_1^{\mathrm{T}}\widehat{\mathbf{R}}_N^{-1}\boldsymbol{e}_1}, \tag{19}$$

is to reconstruct the vector $\mathbf{P}$ with the property (18) such that

$$|\mathbf{W}(z)| = |\mathbf{P}(z)|, \quad \text{for } |z| = 1, p_1 > 0\,. \tag{20}$$

Since the vector $\mathbf{P}$ in (15) specifies the "Maximum Entropy" (ME) spectrum of the p.d. Toeplitz Hermitian matrix, and $\mathbf{W}(z)$ for $|z| = 1$ may be treated as the ME spectrum of the sample matrix $\widehat{\mathbf{R}}_N$, we may state that we intend to reconstruct the p.d. Toeplitz Hermitian matrix, given its sample ME spectrum $\widehat{\mathbf{W}}(z)$. In general, $\widehat{\mathbf{W}}(z)$ may fail to satisfy (18) and may have a number $m < N$ zeros inside the unit disk $|z| < 1$.

In order to find $\mathbf{P}(\mathrm{z})$ that meets (18), the following representation of an arbitrary polynomial $\widehat{\mathbf{W}}(z)$ was used in [11]:

$$\widehat{\mathbf{W}}(z) = b(z)\widehat{\mathbf{P}}(z) \tag{21}$$

where $b(z)$ is a product of elementary factors,

$$b(z) = \prod_{n=1}^{m} \frac{z - z_n}{1 - z_n^* z}, \quad 0 \leq |z| < 1\,, \tag{22}$$

constructed by m zeros of the polynomial $\widehat{\mathbf{W}}(z)$ located inside the unit disk $|z| < 1$, taking multiplicities into account. In (18), $\widehat{\mathbf{P}}(z)$ is the same degree polynomial as $\widehat{\mathbf{W}}(z)$, but with no zeros inside the unit disk $|z| < 1$. With the additional condition $\widehat{\mathbf{P}}_1 = \mathbf{P}(0) > 0$, we have the unique representation:

$$\widehat{\mathbf{P}}(z) = e^{i\gamma} \prod_{n=1}^{m} \frac{1 - z_n^* z}{z - z_n} \widehat{\mathbf{W}}(z), \tag{23}$$

$$\gamma = \pi m + \sum_{n=1}^{m} \arg(z_n)\,. \tag{24}$$

Due to the properties of this product, we have

$$\left|\widehat{\mathbf{P}}(z)\right| = \left|\widehat{\mathbf{W}}(z)\right|, \quad \text{for } |z| = 1 \tag{25}$$

$$\widehat{\mathbf{P}}_1 = \widehat{\mathbf{P}}(0) = \prod_{n=1}^{m} |z_n|^{-1} > 1 \tag{26}$$

since all of the m roots z_n in (25) lie inside the unit disk $|z| < 1$.

Now for the derived vector $\mathbf{P}_N$, using the Gohberg-Semencul theorem [12] we can reconstruct the unique positive definite inverse Hermitian Toeplitz matrix $\widehat{\mathbf{T}}_N^{-1}$:

$$\begin{aligned}\widehat{\mathbf{P}}_1\widehat{\mathbf{T}}_N^{-1} = &\begin{bmatrix} \widehat{\mathbf{P}}_1 & 0 & \cdots & 0 \\ \mathbf{P}_2 & \widehat{\mathbf{P}}_1 & \cdots & 0 \\ \cdots & \cdots & \ddots & 0 \\ \widehat{\mathbf{P}}_N & \widehat{\mathbf{P}}_{N-1} & \cdots & \widehat{\mathbf{P}}_1 \end{bmatrix} \begin{bmatrix} \widehat{\mathbf{P}}_1^* & \mathbf{P}_2^* & \cdots & \mathbf{P}_N^* \\ 0 & \widehat{\mathbf{P}}_1^* & \cdots & \mathbf{P}_{N-1}^* \\ & & \ddots & \\ 0 & 0 & \cdots & \widehat{\mathbf{P}}_1^* \end{bmatrix} \\ &- \begin{bmatrix} 0 & 0 & \cdots & 0 \\ \widehat{\mathbf{P}}_N^* & & & \vdots \\ & \widehat{\mathbf{P}}_N^* & & \vdots \\ & & \ddots & \vdots \\ \widehat{\mathbf{P}}_2^* & \widehat{\mathbf{P}}_3^* & & \widehat{\mathbf{P}}_N^* \; 0 \end{bmatrix} \begin{bmatrix} 0 & \widehat{\mathbf{P}}_N & \cdots & \widehat{\mathbf{P}}_2 \\ & & & \vdots \\ & & \ddots & \widehat{\mathbf{P}}_N \\ 0 & 0 & \cdots & 0 \end{bmatrix}. \end{aligned} \tag{27}$$

Thus, the unique (!) p.d. Toeplitz matrix $\widehat{\mathbf{T}}_N$ has been constructed using the vector $\widehat{\mathbf{W}} = \widehat{\mathbf{R}}_N^{-1}\boldsymbol{e}_1/(\mathbf{e}_1^{\mathrm{T}}\widehat{\mathbf{R}}_N^{-1}\boldsymbol{e}_1)$. We expect that if the phase errors are accurately estimated and compensated so that $\mathbf{Y}_t = \mathbf{X}_t \equiv \mathbf{T}_N{}^{1/2}\boldsymbol{\xi}_t, \boldsymbol{\xi}_t \sim \mathbb{C}\mathcal{N}(0, \mathbf{I}_N)$ in the sample matrix $\widehat{\mathbf{R}}_T = (1/T)\sum_{t=1}^{T} \mathbf{Y}_t\mathbf{Y}_t^{\mathrm{H}}$, then the reconstruction of the Toeplitz matrix from the vector $\widehat{\mathbf{W}} = \widehat{\mathbf{R}}_T^{-1}\boldsymbol{e}_1$ should be close to the true Toeplitz matrix solution. Correspondingly for optimal solutions (with $\widehat{\boldsymbol{\Phi}}_{N-1} \approx \boldsymbol{\Phi}_{N-1}$), we may expect LR values that are close to the scenario-free distribution of the LR calculated for the covariance matrix $\mathbf{T}_N$. If the sample matrix $\widehat{\mathbf{R}}_N(\widehat{\boldsymbol{\Phi}}_{N-1})$ was assembled from the training samples $\mathbf{Y}_t = \mathbf{D}[\boldsymbol{\Phi}_{N-1}]\mathbf{T}_N{}^{1/2}\boldsymbol{\xi}_t$, with $\boldsymbol{\Phi}_{N-1} \neq 0, \boldsymbol{\Phi}_{n-1} \neq (n-1)\theta_o, n = 0,\dots,N-1$, then we may expect significantly smaller $\mathrm{LR}\left(\widehat{\mathbf{R}}_N\middle|\widehat{\mathbf{T}}_N\right)$ values.

Let us investigate the properties of $\mathrm{LR}\left(\widehat{\mathbf{R}}_N\middle|\widehat{\mathbf{T}}_N\right)$ for $\boldsymbol{\Phi}_{N-1} = 0$ for different (N, T). Let us consider the case for N =

17, T = 85, 300, 1000 and calculate $\mathrm{LR}\left(\widehat{\mathbf{R}}_N\middle|\widehat{\mathbf{T}}_N\right)$ and $\mathrm{LR}\left(\widehat{\mathbf{R}}_N\middle|\mathbf{T}_N\right)$, where $\mathbf{T}_N$ is the true covariance matrix and $\widehat{\mathbf{T}}_N$ is the "Gohberg-Semencul" estimate (21)-(27). The true covariance matrix $\mathbf{T}_N$ in calculations of $\mathrm{LR}\left(\widehat{\mathbf{R}}_N\middle|\widehat{\mathbf{T}}_N\right)$ is

$$\begin{aligned}\mathbf{T}_N = q^{-2}\mathbf{I}_N \\ + \mathrm{sinc}\,(W_1) \\ + 0.5\,\mathrm{diag}\,(\theta_o)\,\mathrm{sinc}\,(W_2)\mathrm{diag}^{\mathrm{H}}(\theta_o)\end{aligned} \tag{28}$$

where

$$\mathrm{sinc}\,(W) = \left[\frac{\sin 2\pi W\,(k-l)}{\pi(k-l)}\right]_{k,l=1,N} \tag{29}$$

$$\begin{aligned}\mathrm{diag}(\theta_o) = \mathrm{diag}[1, \exp\left(i\frac{2\pi d}{\lambda}\sin\theta_o\right), \dots, \\ \exp\left(i(N-1)\frac{2\pi d}{\lambda}\sin\theta_o\right)]\end{aligned} \tag{30}$$

$$W_1 = 0.2, W_2 = 0.1, \theta_o = 20^{\mathrm{o}}, q^{-2} = -40\ dB\ .$$

One can see, that for $T \gg N$, the pdf of the sphericity test $\mathrm{LR}\left(\widehat{\mathbf{R}}_N\middle|\widehat{\mathbf{T}}_N\right)$ is quite close to the scenario-invariant pdf of $\mathrm{LR}\left(\widehat{\mathbf{R}}_N\middle|\mathbf{T}_N\right)$.

For small $T \approx N$, the likelihood ratio $\mathrm{LR}\left(\widehat{\mathbf{R}}_N\middle|\widehat{\mathbf{T}}_N\right)$ becomes noticeably smaller than the scenario-invariant values of the sphericity test $\mathrm{LR}\left(\widehat{\mathbf{R}}_N\middle|\mathbf{T}_N\right)$. This divergence of $\mathrm{LR}\left(\widehat{\mathbf{R}}_N\middle|\widehat{\mathbf{T}}_N\right)$ from $\mathrm{LR}\left(\widehat{\mathbf{R}}_N\middle|\mathbf{T}_N\right)$ under the small sample support T condition may be explained by the absence of random matrix theory (RMT) consistency in the sample matrix eigenvalues under a small sample support. Note in this regard that as demonstrated in [13], the "calibration" phase estimation problem belongs to the class of adaptive problems with strong convergence that for accurate estimation requires an asymptotically large sample support. This is opposed to adaptive problems with "criterion" convergence, such as adaptive beamforming for external noise source mitigation [14]. In [5], the minimal sample support T_{min} is defined as $T_{min} > N^2$, for example. And yet, we may expect that the RMT modification of the sample matrix $\widehat{\mathbf{R}}_N$ eigenvalues may improve $\mathrm{LR}\left(\widehat{\mathbf{R}}_N\middle|\widehat{\mathbf{T}}_N\right)$ values, bringing it closer to the scenario-invariant $\mathrm{LR}\left(\widehat{\mathbf{R}}_N\middle|\mathbf{T}_N\right)$ values.

According to Theorem 3 in [15], the following quantities are strongly (T, N) consistent:

$$\hat{\gamma}_n = \frac{T}{K_n}\sum_{K\in\varkappa_n}(\hat{\lambda}_k - \hat{\mu}_k) \tag{31}$$

where $\hat{\lambda}_k$ is the traditional k-th eigenvalue with multiplicity $\varkappa_k$ and $\hat{\mu}_1 < \hat{\mu}_2 < \cdots < \hat{\mu}_N$ are the real-valued solutions to the following problem:

$$\frac{1}{N}\sum_{K=1}^{N}\frac{\hat{\lambda}_k}{\hat{\lambda}_k - \hat{\mu}} = \frac{1}{C},\quad C = \frac{N}{T} < 1\,. \tag{32}$$

Therefore, given the eigenvalues of the sample matrix $\widehat{\mathbf{R}}_N$ ($\hat{\lambda}_1 \le \hat{\lambda}_2 \le \cdots \le \hat{\lambda}_N$), we may modify the sample eigenvalues by replacing $\hat{\lambda}_j$ by $\hat{\gamma}_j$ and use this new sample matrix $\widehat{\mathbf{R}}_N$ for finding the Toeplitz matrix $\widehat{\mathbf{T}}_N$. It is expected that since the RMT eigenvalues modification (31)-(32) reduces the eigenvalue's dynamic range

$$\frac{\hat{\lambda}_{\max}}{\hat{\lambda}_{\min}} > \frac{\hat{\gamma}_{\max}}{\hat{\gamma}_{\min}}, \tag{33}$$

this modification should also change the dynamic range of the ME spectrum, and therefore should improve the reconstructed Toeplitz matrix $\widehat{\mathbf{T}}_N$ and the likelihood ratio (sphericity test) $\mathrm{LR}\left(\widehat{\mathbf{R}}_N^m\middle|\widehat{\mathbf{T}}_N^m\right)$ for the modified matrices, $\widehat{\mathbf{R}}_N^m$ and $\widehat{\mathbf{T}}_N^m$. In Fig. 1-Fig. 5, we introduce the sample pdf's for the RMT-modified eigenspectrum of the sample matrix in accordance with Theorem 3 [15].

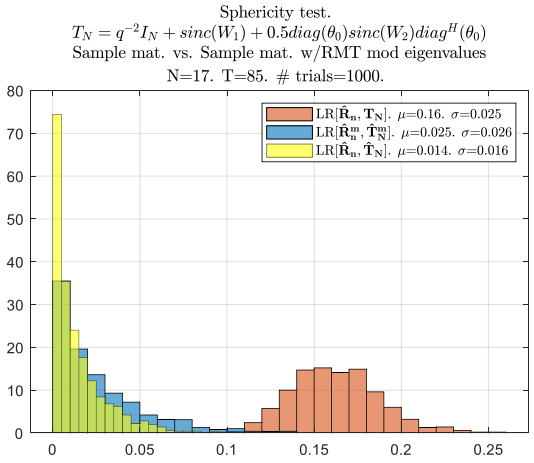

Fig. 1.Sphericity test of 1) $LR\left(\widehat{\boldsymbol{R}}_N\middle|\boldsymbol{T}_N\right)$: sample matrix ($\widehat{\boldsymbol{R}}_N$) & true covariance matrix ($\boldsymbol{T}_N$) 2) $LR\left(\widehat{\boldsymbol{R}}_N^m\middle|\widehat{\boldsymbol{T}}_N^m\right)$: sample matrix with RMT modified eigenvalues ($\widehat{\boldsymbol{R}}_N^m$) & its Gohberg-Semencul estimate ($\widehat{\boldsymbol{T}}_N^m$), 3) $LR\left(\widehat{\boldsymbol{R}}_N\middle|\widehat{\boldsymbol{T}}_N\right)$: sample matrix ($\widehat{\boldsymbol{R}}_N$) & its Gohberg-Semencul estimate ($\widehat{\boldsymbol{T}}_N$), where $\boldsymbol{T}_N = q^{-2}\boldsymbol{I}_N + \mathrm{sinc}\,(W_1) + 0.5\,\mathrm{diag}\,(\theta_o)\,\mathrm{sinc}\,(W_2)\mathrm{diag}^{\mathrm{H}}(\theta_o)$. N=17, T=85, 1000 trials.

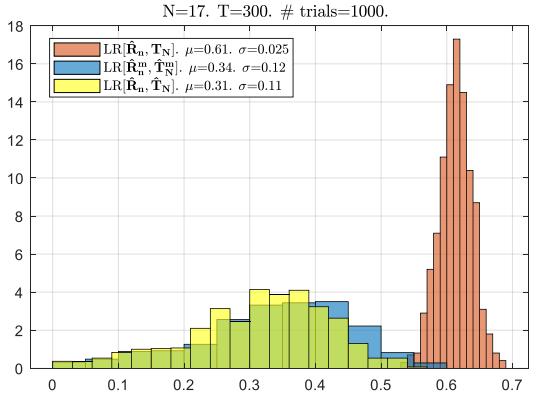

Fig. 2. Sphericity test of 1) $LR\left(\widehat{\boldsymbol{R}}_N\middle|\boldsymbol{T}_N\right)$: sample matrix ($\widehat{\boldsymbol{R}}_N$) & true covariance matrix ($\boldsymbol{T}_N$) 2) $LR\left(\widehat{\boldsymbol{R}}_N^m\middle|\widehat{\boldsymbol{T}}_N^m\right)$: sample matrix with RMT modified eigenvalues ($\widehat{\boldsymbol{R}}_N^m$) & its Gohberg-Semencul estimate ($\widehat{\boldsymbol{T}}_N^m$), 3) $LR\left(\widehat{\boldsymbol{R}}_N\middle|\widehat{\boldsymbol{T}}_N\right)$:

sample matrix ($\widehat{\boldsymbol{R}}_{\boldsymbol{N}}$) & its Gohberg-Semencul estimate ($\widehat{\boldsymbol{T}}_{\boldsymbol{N}}$), where $\boldsymbol{T}_N = q^{-2}\boldsymbol{I}_N + \text{sinc}\,(W_1) + \ 0.5\ \text{diag}\,(\theta_o)\ \text{sinc}\,(W_2)\text{diag}^{\text{H}}(\theta_o)$. N=17, T=300, 1000 trials.

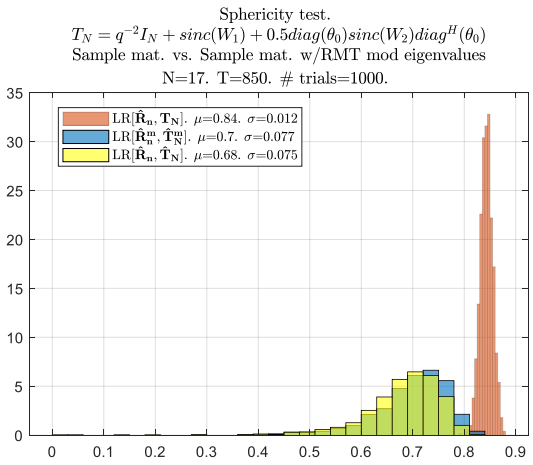

Fig. 3. Sphericity test of 1) $LR\left(\widehat{\boldsymbol{R}}_{\boldsymbol{N}}\middle|\boldsymbol{T}_{\boldsymbol{N}}\right)$: sample matrix ($\widehat{\boldsymbol{R}}_{\boldsymbol{N}}$) & true covariance matrix ($\boldsymbol{T}_{\boldsymbol{N}}$) 2) $LR\left(\widehat{\boldsymbol{R}}_{\boldsymbol{N}}^{\boldsymbol{m}}\middle|\widehat{\boldsymbol{T}}_{\boldsymbol{N}}^{\boldsymbol{m}}\right)$: sample matrix with RMT modified eigenvalues ($\widehat{\boldsymbol{R}}_{\boldsymbol{N}}^{\boldsymbol{m}}$) & its Gohberg-Semencul estimate ($\widehat{\boldsymbol{T}}_{\boldsymbol{N}}^{\boldsymbol{m}}$), 3) $LR\left(\widehat{\boldsymbol{R}}_{\boldsymbol{N}}\middle|\widehat{\boldsymbol{T}}_{\boldsymbol{N}}\right)$: sample matrix ($\widehat{\boldsymbol{R}}_{\boldsymbol{N}}$) & its Gohberg-Semencul estimate ($\widehat{\boldsymbol{T}}_{\boldsymbol{N}}$), where $\boldsymbol{T}_N = q^{-2}\boldsymbol{I}_N + \text{sinc}\,(W_1) + \ 0.5\ \text{diag}\,(\theta_o)\ \text{sinc}\,(W_2)\text{diag}^{\text{H}}(\theta_o)$. N=17, T=850, 1000 trials.

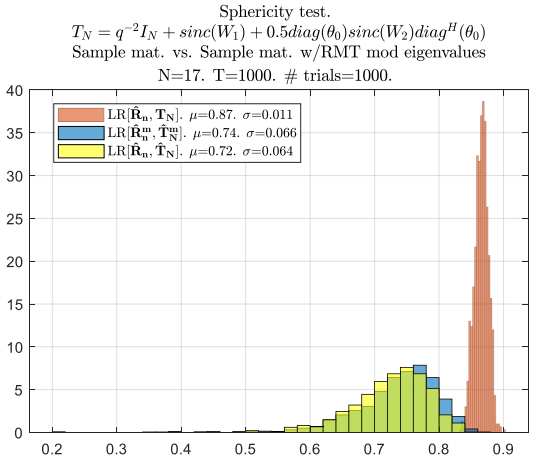

Fig. 4. Sphericity test of 1) $\text{LR}\left(\widehat{\mathbf{R}}_{\mathbf{N}}\middle|\mathbf{T}_{\mathbf{N}}\right)$: sample matrix ($\widehat{\mathbf{R}}_{\mathbf{N}}$) & true covariance matrix ($\mathbf{T}_{\mathbf{N}}$) 2) $\text{LR}\left(\widehat{\mathbf{R}}_{\mathbf{N}}^{\mathbf{m}}\middle|\widehat{\mathbf{T}}_{\mathbf{N}}^{\mathbf{m}}\right)$: sample matrix with RMT modified eigenvalues ($\widehat{\mathbf{R}}_{\mathbf{N}}^{\mathbf{m}}$) & its Gohberg-Semencul estimate ($\widehat{\mathbf{T}}_{\mathbf{N}}^{\mathbf{m}}$), 3) $\text{LR}\left(\widehat{\mathbf{R}}_{\mathbf{N}}\middle|\widehat{\mathbf{T}}_{\mathbf{N}}\right)$: sample matrix ($\widehat{\mathbf{R}}_{\mathbf{N}}$) & its Gohberg-Semencul estimate ($\widehat{\mathbf{T}}_{\mathbf{N}}$), where $\mathbf{T}_{\text{N}} = \text{q}^{-2}\mathbf{I}_{\text{N}} + \text{sinc}\,(\text{W}_1) + \ 0.5\ \text{diag}\,(\theta_o)\ \text{sinc}\,(\text{W}_2)\text{diag}^{\text{H}}(\theta_o)$. N=17, T=1000, 1000 trials.

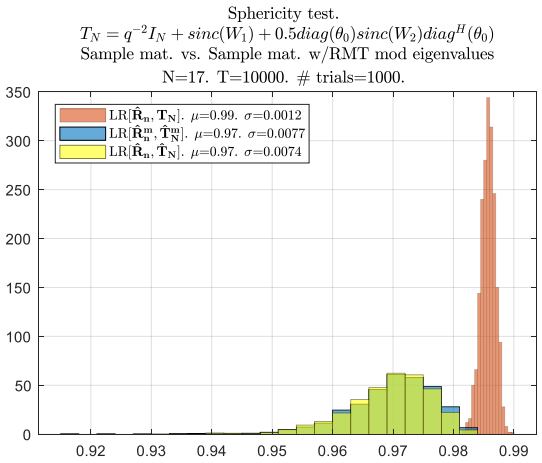

Fig. 5 Sphericity test of 1) $\text{LR}\left(\widehat{\mathbf{R}}_{\text{N}}\middle|\mathbf{T}_{\text{N}}\right)$: sample matrix ($\widehat{\mathbf{R}}_{\mathbf{N}}$) & true covariance matrix ($\mathbf{T}_{\text{N}}$) 2) $\text{LR}\left(\widehat{\mathbf{R}}_{\text{N}}^{\text{m}}\middle|\widehat{\mathbf{T}}_{\text{N}}^{\text{m}}\right)$: sample matrix with RMT modified eigenvalues ($\widehat{\mathbf{R}}_{\mathbf{N}}^{\mathbf{m}}$) & its Gohberg-Semencul estimate ($\widehat{\mathbf{T}}_{\mathbf{N}}^{\mathbf{m}}$), 3) $\text{LR}\left(\widehat{\mathbf{R}}_{\text{N}}\middle|\widehat{\mathbf{T}}_{\text{N}}\right)$: sample matrix ($\widehat{\mathbf{R}}_{\mathbf{N}}$) & its Gohberg-Semencul estimate ($\widehat{\mathbf{T}}_{\mathbf{N}}$), where $\mathbf{T}_{\text{N}} = \text{q}^{-2}\mathbf{I}_{\text{N}} + \text{sinc}\,(\text{W}_1) + \ 0.5\ \text{diag}\,(\theta_o)\ \text{sinc}\,(\text{W}_2)\text{diag}^{\text{H}}(\theta_o)$. N=17, T=10000, 1000 trials.

As one can see, the RMT eigenvalues modification significantly extends the sample support values T whereby the pdf's for $\text{LR}\left(\widehat{\mathbf{R}}_{\boldsymbol{N}}\middle|\mathbf{T}_{\boldsymbol{N}}\right)$ overlap with the LR for the modified matrices $\text{LR}\left(\widehat{\mathbf{R}}_{\boldsymbol{N}}^{\boldsymbol{m}}\middle|\widehat{\mathbf{T}}_{\boldsymbol{N}}^{\boldsymbol{m}}\right)$.

Finally, let us introduce the similar set of sample pdf's calculated for a different true covariance Toeplitz matrix $\mathbf{T}_N$:

$$\mathbf{T}_N = q^{-2}\mathbf{I}_N + \text{sinc}\,(W_1)\,. \tag{34}$$

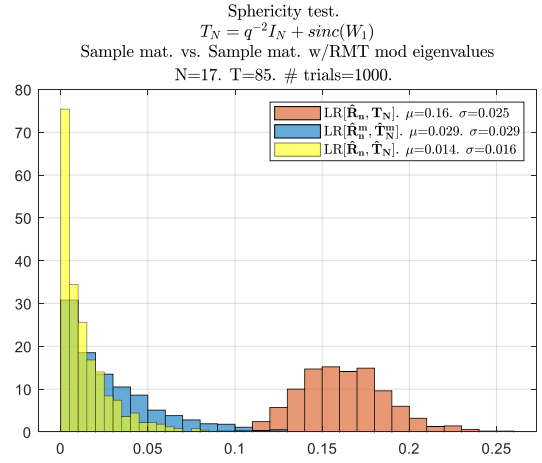

Fig. 6. Sphericity test of 1) $LR\left(\widehat{\boldsymbol{R}}_{\boldsymbol{N}}\middle|\boldsymbol{T}_{\boldsymbol{N}}\right)$: sample matrix ($\widehat{\boldsymbol{R}}_{\boldsymbol{N}}$) & true covariance matrix ($\boldsymbol{T}_{\boldsymbol{N}}$) 2) $LR\left(\widehat{\boldsymbol{R}}_{\boldsymbol{N}}^{\boldsymbol{m}}\middle|\widehat{\boldsymbol{T}}_{\boldsymbol{N}}^{\boldsymbol{m}}\right)$: sample matrix with RMT modified eigenvalues ($\widehat{\boldsymbol{R}}_{\boldsymbol{N}}^{\boldsymbol{m}}$) & its Gohberg-Semencul estimate ($\widehat{\boldsymbol{T}}_{\boldsymbol{N}}^{\boldsymbol{m}}$), 3) $LR\left(\widehat{\boldsymbol{R}}_{\boldsymbol{N}}\middle|\widehat{\boldsymbol{T}}_{\boldsymbol{N}}\right)$: sample matrix ($\widehat{\boldsymbol{R}}_{\boldsymbol{N}}$) & its Gohberg-Semencul estimate ($\widehat{\boldsymbol{T}}_{\boldsymbol{N}}$), where $\boldsymbol{T}_N = q^{-2}\boldsymbol{I}_N + \text{sinc}\,(W_1)$. N=17, T=85, 1000 trials.

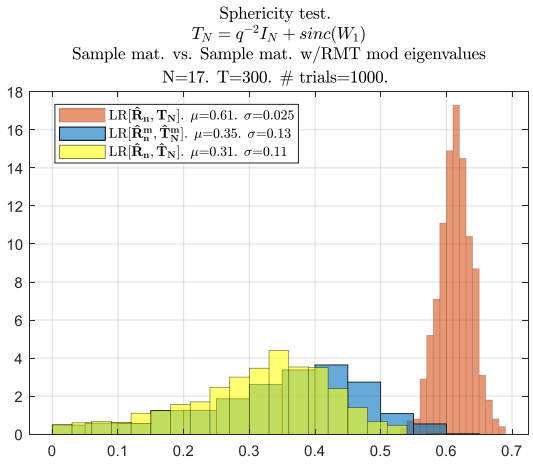

Fig. 7. Sphericity test of 1) $LR(\hat{\boldsymbol{R}}_N|\boldsymbol{T}_N)$: sample matrix ($\hat{\boldsymbol{R}}_N$) & true covariance matrix ($\boldsymbol{T}_N$) 2) $LR(\hat{\boldsymbol{R}}_N^m|\hat{\boldsymbol{T}}_N^m)$: sample matrix with RMT modified eigenvalues ($\hat{\boldsymbol{R}}_N^m$) & its Gohberg-Semencul estimate ($\hat{\boldsymbol{T}}_N^m$), 3) $LR(\hat{\boldsymbol{R}}_N|\hat{\boldsymbol{T}}_N)$: sample matrix ($\hat{\boldsymbol{R}}_N$) & its Gohberg-Semencul estimate ($\hat{\boldsymbol{T}}_N$), where $\boldsymbol{T}_N = q^{-2}\boldsymbol{I}_N + \text{sinc}\,(W_1)$. N=17, T=300, 1000 trials.

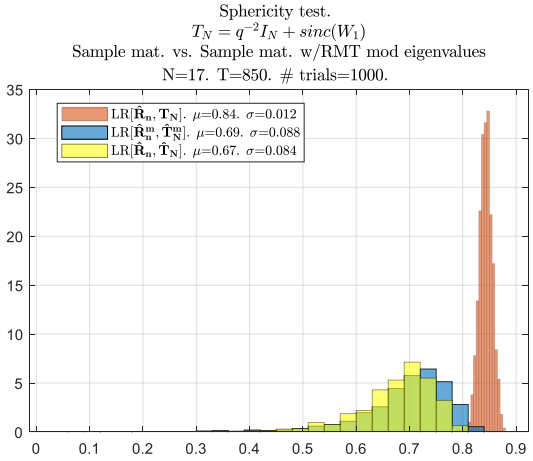

Fig. 8. Sphericity test of 1) $LR(\hat{\boldsymbol{R}}_N|\boldsymbol{T}_N)$: sample matrix ($\hat{\boldsymbol{R}}_N$) & true covariance matrix ($\boldsymbol{T}_N$) 2) $LR(\hat{\boldsymbol{R}}_N^m|\hat{\boldsymbol{T}}_N^m)$: sample matrix with RMT modified eigenvalues ($\hat{\boldsymbol{R}}_N^m$) & its Gohberg-Semencul estimate ($\hat{\boldsymbol{T}}_N^m$), 3) $LR(\hat{\boldsymbol{R}}_N|\hat{\boldsymbol{T}}_N)$: sample matrix ($\hat{\boldsymbol{R}}_N$) & its Gohberg-Semencul estimate ($\hat{\boldsymbol{T}}_N$), where $\boldsymbol{T}_N = q^{-2}\boldsymbol{I}_N + \text{sinc}\,(W_1)$. N=17, T=850, 1000 trials.

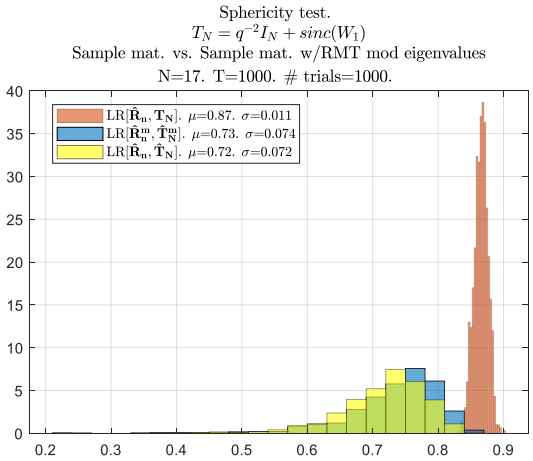

Fig. 9. Sphericity test of 1) $LR(\hat{\boldsymbol{R}}_N|\boldsymbol{T}_N)$: sample matrix ($\hat{\boldsymbol{R}}_N$) & true covariance matrix ($\boldsymbol{T}_N$) 2) $LR(\hat{\boldsymbol{R}}_N^m|\hat{\boldsymbol{T}}_N^m)$: sample matrix with RMT modified eigenvalues ($\hat{\boldsymbol{R}}_N^m$) & its Gohberg-Semencul estimate ($\hat{\boldsymbol{T}}_N^m$), 3) $LR(\hat{\boldsymbol{R}}_N|\hat{\boldsymbol{T}}_N)$: sample matrix ($\hat{\boldsymbol{R}}_N$) & its Gohberg-Semencul estimate ($\hat{\boldsymbol{T}}_N$), where $\boldsymbol{T}_N = q^{-2}\boldsymbol{I}_N + \text{sinc}\,(W_1)$. N=17, T=1000, 1000 trials.

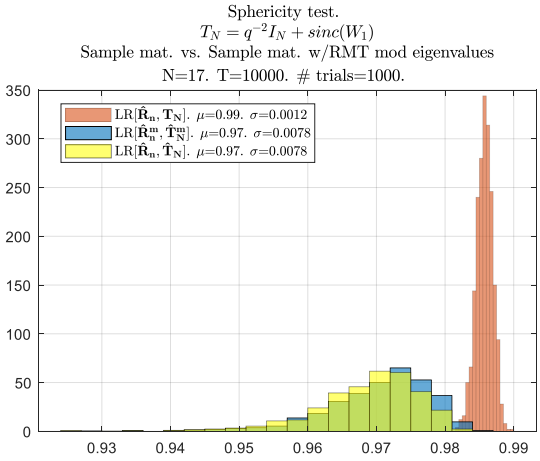

Fig. 10. Sphericity test of 1) $LR(\hat{\boldsymbol{R}}_N|\boldsymbol{T}_N)$: sample matrix ($\hat{\boldsymbol{R}}_N$) & true covariance matrix ($\boldsymbol{T}_N$) 2) $LR(\hat{\boldsymbol{R}}_N^m|\hat{\boldsymbol{T}}_N^m)$: sample matrix with RMT modified eigenvalues ($\hat{\boldsymbol{R}}_N^m$) & its Gohberg-Semencul estimate ($\hat{\boldsymbol{T}}_N^m$), 3) $LR(\hat{\boldsymbol{R}}_N|\hat{\boldsymbol{T}}_N)$: sample matrix ($\hat{\boldsymbol{R}}_N$) & its Gohberg-Semencul estimate ($\hat{\boldsymbol{T}}_N$), where $\boldsymbol{T}_N = q^{-2}\boldsymbol{I}_N + \text{sinc}\,(W_1)$. N=17, T=10000, 1000 trials.

One can see, that for hypotheses H_1, the sample pdf's remain practically the same for both Toeplitz matrices (29) and (34).

Let us now analyze the LR behavior for the hypothesis H_0, when the true covariance matrix $\mathbf{R}_N$ is not a p.d. Toeplitz Hermitian matrix. Specifically, we consider the case when the antenna is not properly calibrated and

$$\mathbf{R}_N = \mathbf{D}[\boldsymbol{\Phi}_{N-1}]\mathbf{T}_N\mathbf{D}^{\mathrm{H}}[\boldsymbol{\Phi}_{N-1}]\,, \tag{35}$$

where the phase errors φ_n in $\mathbf{D}[\boldsymbol{\Phi}_{N-1}]$ are i.i.d. random values, uniformly distributed within the range

$$-\varphi_{\max} \le \varphi_n \le \varphi_{\max} \tag{36}$$

for the different $\varphi_{\max} \le \pi$ values. As follows from Fig. 11-Fig. 15 of pdf's, for N = 17, T = 300, even a very small calibration phase error $\varphi_{max} \le 2^{\circ}$ leads to a dramatic LR degradation so that the sample pdf's of the LR do not line up with the pdf's of the $\text{LR}(\hat{\mathbf{R}}_N^m|\hat{\mathbf{T}}_N^m)$ calculated for the hypothesis H_1 with $\varphi_l = 0$. Note that for $T > 300$, using the RMT-modified Toeplitz matrix estimates in $\text{LR}(\hat{\mathbf{R}}_N^m|\hat{\mathbf{T}}_N^m)$ allows for using the modified scenario-invariant pdf's $\text{LR}(\hat{\mathbf{R}}_N|\mathbf{T}_N)$ for the threshold estimation without significant losses in performance. Therefore, the sphericity test with the Gohberg-Semencul restoration of a p.d. Toeplitz matrix, given the RMT-modified sample matrix $\hat{\mathbf{R}}_N^m$, allows for reliable identification of a poorly calibrated antenna array and may be used for validation of the ULA calibration accuracy.

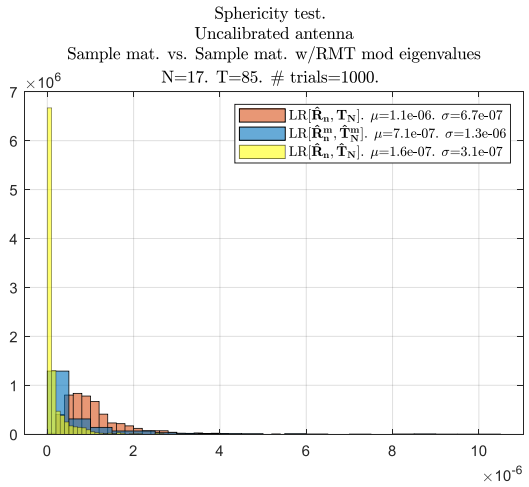

Fig. 11. Sphericity test of 1) $LR(\widehat{\boldsymbol{R}}_N|\boldsymbol{T}_N)$: sample matrix ($\widehat{\boldsymbol{R}}_N$) & true covariance matrix ($\boldsymbol{T}_N$) 2) $LR(\widehat{\boldsymbol{R}}_N^m|\widehat{\boldsymbol{T}}_N^m)$: sample matrix with RMT modified eigenvalues ($\widehat{\boldsymbol{R}}_N^m$) & its Gohberg-Semencul estimate ($\widehat{\boldsymbol{T}}_N^m$), 3) $LR(\widehat{\boldsymbol{R}}_N|\widehat{\boldsymbol{T}}_N)$: sample matrix ($\widehat{\boldsymbol{R}}_N$) & its Gohberg-Semencul estimate ($\widehat{\boldsymbol{T}}_N$), with an uncalibrated antenna. N=17, T=85, 1000 trials.

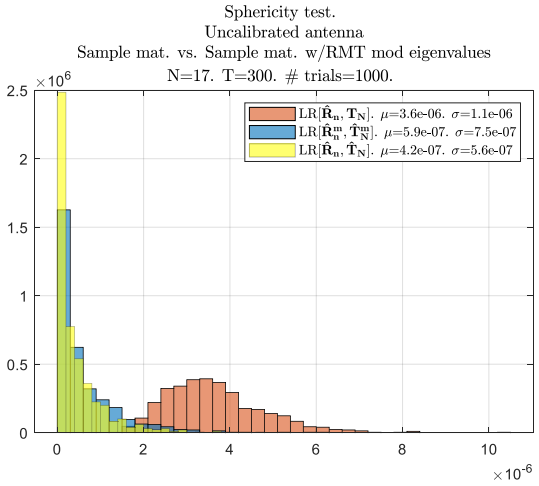

Fig. 12. Sphericity test of 1) $LR(\widehat{\boldsymbol{R}}_N|\boldsymbol{T}_N)$: sample matrix ($\widehat{\boldsymbol{R}}_N$) & true covariance matrix ($\boldsymbol{T}_N$) 2) $LR(\widehat{\boldsymbol{R}}_N^m|\widehat{\boldsymbol{T}}_N^m)$: sample matrix with RMT modified eigenvalues ($\widehat{\boldsymbol{R}}_N^m$) & its Gohberg-Semencul estimate ($\widehat{\boldsymbol{T}}_N^m$), 3) $LR(\widehat{\boldsymbol{R}}_N|\widehat{\boldsymbol{T}}_N)$: sample matrix ($\widehat{\boldsymbol{R}}_N$) & its Gohberg-Semencul estimate ($\widehat{\boldsymbol{T}}_N$), with an uncalibrated antenna. N=17, T=300, 1000 trials.

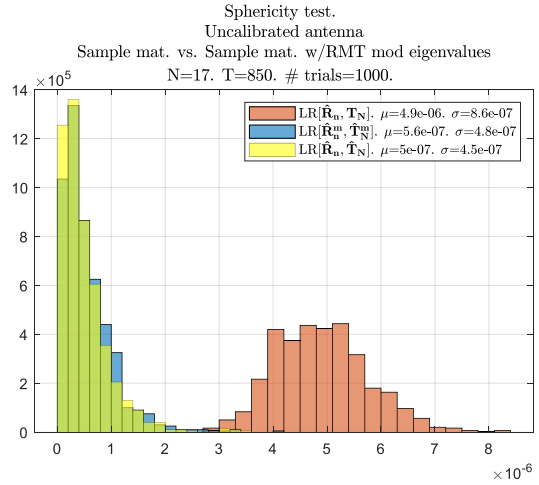

Fig. 13. Sphericity test of 1) $LR(\widehat{\boldsymbol{R}}_N|\boldsymbol{T}_N)$: sample matrix ($\widehat{\boldsymbol{R}}_N$) & true covariance matrix ($\boldsymbol{T}_N$) 2) $LR(\widehat{\boldsymbol{R}}_N^m|\widehat{\boldsymbol{T}}_N^m)$: sample matrix with RMT modified eigenvalues ($\widehat{\boldsymbol{R}}_N^m$) & its Gohberg-Semencul estimate ($\widehat{\boldsymbol{T}}_N^m$), 3) $LR(\widehat{\boldsymbol{R}}_N|\widehat{\boldsymbol{T}}_N)$: sample matrix ($\widehat{\boldsymbol{R}}_N$) & its Gohberg-Semencul estimate ($\widehat{\boldsymbol{T}}_N$), with an uncalibrated antenna. N=17, T=850, 1000 trials.

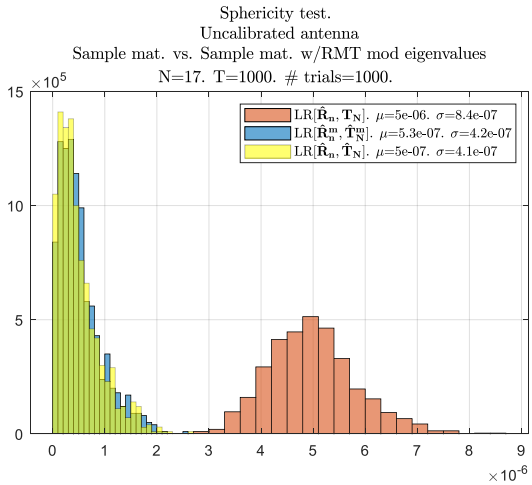

Fig. 14. Sphericity test of 1) $LR(\widehat{\boldsymbol{R}}_N|\boldsymbol{T}_N)$: sample matrix ($\widehat{\boldsymbol{R}}_N$) & true covariance matrix ($\boldsymbol{T}_N$) 2) $LR(\widehat{\boldsymbol{R}}_N^m|\widehat{\boldsymbol{T}}_N^m)$: sample matrix with RMT modified eigenvalues ($\widehat{\boldsymbol{R}}_N^m$) & its Gohberg-Semencul estimate ($\widehat{\boldsymbol{T}}_N^m$), 3) $LR(\widehat{\boldsymbol{R}}_N|\widehat{\boldsymbol{T}}_N)$: sample matrix ($\widehat{\boldsymbol{R}}_N$) & its Gohberg-Semencul estimate ($\widehat{\boldsymbol{T}}_N$), with an uncalibrated antenna. N=17, T=1000, 1000 trials.

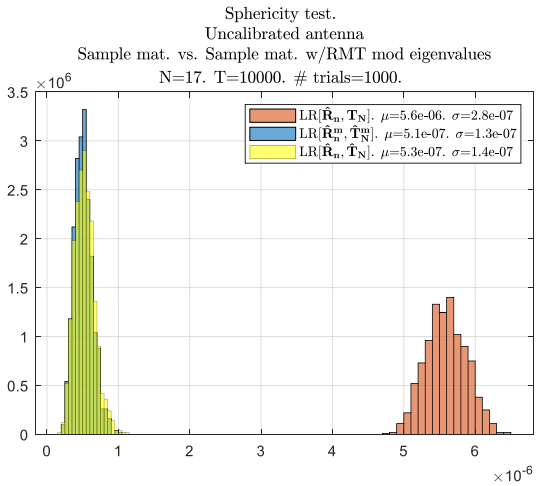

Fig. 15. Sphericity test of 1) $LR(\widehat{\boldsymbol{R}}_N|\boldsymbol{T}_N)$: sample matrix ($\widehat{\boldsymbol{R}}_N$) & true covariance matrix ($\boldsymbol{T}_N$) 2) $LR(\widehat{\boldsymbol{R}}_N^m|\widehat{\boldsymbol{T}}_N^m)$: sample matrix with RMT modified eigenvalues ($\widehat{\boldsymbol{R}}_N^m$) & its Gohberg-Semencul estimate ($\widehat{\boldsymbol{T}}_N^m$), 3) $LR(\widehat{\boldsymbol{R}}_N|\widehat{\boldsymbol{T}}_N)$: sample matrix ($\widehat{\boldsymbol{R}}_N$) & its Gohberg-Semencul estimate ($\widehat{\boldsymbol{T}}_N$), with an uncalibrated antenna. N=17, T=10000, 1000 trials.

III. Cramer-Rao and ML Calibration Phase Estimation for the Benchmark Scenario

As a benchmark we consider the scenario with the a priori known Toeplitz covariance matrix analyzed in [16]. Obviously, the efficiency of the phase calibration in this scenario should be compared with the efficiency of the techniques proposed below for conditions with the a priori not known or partly known covariance Toeplitz matrix. Moreover, as discussed in Introduction, in active HF OTHR mode and appropriate propagation conditions, the spatial covariance matrix of the clutter return may be specified by the beampattern of the Tx antenna and may be treated as known a priori. The need to come

back to this analysis, conducted in [16], is due to some novel results derived below.

Let us start from the derivation of the formula for the Cramer-Rao Bound (CRB) calculation. The (*n*, *m*)-th element of the Fisher information matrix (FIM) is found using the traditional formula:

$$\mathbf{J}_{nm} = T\,\mathrm{Tr}[\mathbf{R}_n\mathbf{R}_N^{-1}\mathbf{R}_m\mathbf{R}_N^{-1}] \tag{37}$$

where

$$\mathbf{R}_n = \frac{\partial \mathbf{R}_N}{\partial \varphi_n}. \tag{38}$$

Since

$$\begin{aligned}\frac{\partial \mathbf{R}_N}{\partial \varphi_n} &= \frac{\partial \mathbf{D}[\mathbf{\Phi}_{N-1}]}{\partial \varphi_n}\mathbf{T}_N\mathbf{D}^{\mathrm{H}}[\mathbf{\Phi}_{N-1}] \\ &\quad + \mathbf{D}[\mathbf{\Phi}_{N-1}]\mathbf{T}_N^{-1}\frac{\partial \mathbf{D}^{\mathrm{H}}[\mathbf{\Phi}_{N-1}]}{\partial \varphi_n}\end{aligned} \tag{39}$$

we get

$$\begin{aligned}\frac{\partial \mathbf{R}_N}{\partial \varphi_n} &= \mathrm{diag}[0,\dots,i\exp(i\varphi_n),0,\dots,0]\mathbf{T}_N\mathbf{D}^{\mathrm{H}}[\mathbf{\Phi}_{N-1}] \\ &\quad + \mathbf{D}[\mathbf{\Phi}_{N-1}]\mathbf{T}_N^{-1} \\ &\quad \times \mathrm{diag}[0,\dots,-i\exp(-i\varphi_n),0,\dots,0],\end{aligned} \tag{40}$$

and then

$$\begin{aligned}\mathbf{R}_N^{-1}\mathbf{R}_n\mathbf{R}_N^{-1} &= \mathbf{R}_N^{-1}\mathrm{diag}[0,\dots,0,-i,0,\dots,0] \\ &\quad + \mathrm{diag}[0,\dots,0,i,0,\dots 0]\mathbf{R}_N^{-1},\end{aligned} \tag{41}$$

which finally leads to

$$\begin{aligned}\mathbf{R}_N^{-1}\mathbf{R}_n\mathbf{R}_N^{-1} &= iC_n \\ &= i\begin{bmatrix} 0 & \dots & 0 & r^{1n} & 0 & \dots & 0 \\ \vdots & & & \vdots & & & \\ -r^{n1} & \dots & & 0 & & \dots & -r^{nN} \\ \vdots & & & \vdots & & & \\ 0 & \dots & 0 & r^{Nn} & 0 & \dots & 0 \end{bmatrix}.\end{aligned} \tag{42}$$

Here $(r^{1n}, r^{2n}, \dots, r^{Nn})$ are the elements of the *n*-th column of the inverse matrix $\mathbf{R}_N^{-1}$; $(-r^{n1}, -r^{n2}, \dots, -r^{nN})$ are the elements of the *n*-th row of the matrix $\mathbf{R}_N^{-1}$ with the inverted sign. Note that the diagonal element r^{nn} is missing in (42). With respect to (42), we get

$$\begin{aligned}\mathbf{R}_N^{-1}\mathbf{R}_n\mathbf{R}_N^{-1}\mathbf{R}_m &= i^2C_n \\ &\quad \times \{[\mathrm{diag}[0,\dots,0,\exp(i\varphi_m),0,\dots,0] \\ &\quad \times \mathbf{T}_N\mathbf{D}^{\mathrm{H}}(\mathbf{\Phi}_{N-1}) - \mathbf{D}(\mathbf{\Phi}_{N-1})\mathbf{T}_N \\ &\quad \times \mathrm{diag}[0,\dots,0,\exp(-i\varphi_m),0,\dots,0]]\}\end{aligned} \tag{43}$$

or

$$\mathbf{R}_N^{-1}\mathbf{R}_n\mathbf{R}_N^{-1}\mathbf{R}_m = i^2C_n\left[\mathrm{diag}\left[0,\dots,0,\overset{m}{\widehat{1}},0,\dots,0\right]\mathbf{R}_N - \mathbf{R}_N\mathrm{diag}\left[0,\dots,0,\overset{m}{\widehat{1}},0,\dots,0\right]\right]. \tag{44}$$

Correspondingly, for $\mathrm{Tr}[\mathbf{R}_N^{-1}\mathbf{R}_n\mathbf{R}_N^{-1}\mathbf{R}_m]$ we have

$$\begin{aligned}&\mathrm{Tr}[\mathbf{R}_N^{-1}\mathbf{R}_n\mathbf{R}_N^{-1}\mathbf{R}_m] = \\ &\quad \mathrm{Tr}\,C_n\left\{\begin{bmatrix} 0 & \cdots & 0 \\ \vdots & \cdots & \vdots \\ -r_{m1} & \cdots & -r_{mN} \\ \vdots & \cdots & \vdots \\ 0 & \cdots & 0 \end{bmatrix}\right. \\ &\quad \left. + \begin{bmatrix} 0 & \cdots & 0 & r^{1n} & 0 & \cdots & 0 \\ \vdots & & & \vdots & & & \\ 0 & \cdots & 0 & r^{Nn} & 0 & \cdots & 0 \end{bmatrix}\right\}\end{aligned} \tag{45}$$

$$\begin{aligned}&= \mathrm{Tr}\left\{\begin{pmatrix} 0 & \cdots & 0 & r^{1n} & 0 & \cdots & 0 \\ \vdots & & & \vdots & & & \vdots \\ -r^{n1} & \cdots & & 0 & & \cdots & -r^{nN} \\ \vdots & & & \vdots & & & \vdots \\ 0 & \cdots & 0 & r^{Nn} & 0 & \cdots & 0 \end{pmatrix}\right. \\ &\quad \left.\times\begin{pmatrix} 0 & \cdots & 0 & r_{1m} & 0 & \cdots & 0 \\ \vdots & & & \vdots & & & \vdots \\ -r_{m1} & \cdots & & 0 & & \cdots & -r_{mN} \\ \vdots & & & \vdots & & & \vdots \\ 0 & \cdots & 0 & r_{Nm} & 0 & \cdots & 0 \end{pmatrix}\right\} \\ &\quad \text{for n=m} \\ &= 0, \quad \text{for } n \neq m.\end{aligned} \tag{46}$$

From (46), for $n = m$ we have:

$$\mathrm{Tr}[\mathbf{R}_N^{-1}\mathbf{R}_n\mathbf{R}_N^{-1}\mathbf{R}_m] = 2(r^{nn}r_{nn} - 1). \tag{47}$$

Correspondingly, for the Cramer-Rao Bound we have

$$\mathrm{CRB}(\varphi_n) = \frac{1}{2T[(\mathbf{T}_N^{-1})_{nn}(\mathbf{T}_N)_{nn} - 1]}. \tag{48}$$

Note, that (48) is a new and simpler expression than the one introduced in [15]. Yet, despite its simplicity, the expression provides an important insight into the ML phase errors estimation potential (benchmark) accuracy.

One can see that for $\mathbf{T}_N \to \sigma_n^2\mathbf{I}_N$, i.e. when the signal covariance matrix tends to the white noise matrix, no phase errors estimation is possible since $\mathrm{CRB}(\varphi_n) \to \infty$. On the other hand, if $\lambda_{min}[\mathbf{T}_N] \to 0$, then the product $r^{nn}r_{nn} \to \infty$, which means the potential phase calibration errors tend to zero. Therefore, the large clutter-to-internal noise ratio is the necessary condition for efficient antenna calibration. Moreover, since for the Toeplitz matrix all elements r_{nn} on the main diagonal are the same, the best accuracy may be expected for the antenna elements with the maximal $(\mathbf{T}_N^{-1})_{nn}$ values, which are usually the central elements of the array. Numerical accuracy of the derived CRB for the ML estimation will be explored in the next section where we investigate the efficiency of some "invariant" phase errors estimation techniques. In this

section, let us re-derive the ML estimation algorithm and introduce the "invariant" phase errors estimation techniques that do not require knowledge of the Toeplitz covariance matrix. For the a priori known Toeplitz covariance matrix $\mathbf{T}_N$, the estimated Hermitian covariance matrix $\mathbf{R}_N$ is represented as (8)

$$\mathbf{R}_N = \mathbf{D}[\mathbf{\Phi}_{N-1}]\mathbf{T}_N\mathbf{D}^{\mathrm{H}}[\mathbf{\Phi}_{N-1}] \tag{49}$$

where

$$\mathbf{T}_N = q_n^{-2}\mathbf{I}_o + \mathbf{T}_N^o \tag{50}$$

and

$$\mathbf{D}(\mathbf{\Phi}_{N-1}) = \mathrm{diag}[1, e^{i\varphi_1}, \dots, e^{i\varphi_{N-1}}] \tag{51}$$

where $\boldsymbol{\varphi}_j, j = 1, \dots, N-1$ are the unknown "calibration" phase errors, uniformly distributed within the interval

$$-\varphi_{\max} \le \varphi \le \varphi_{\max},\ \ \varphi_{\max} \le \pi\,. \tag{52}$$

For the i.i.d. Gaussian training data $\mathbf{x}_t, t = 1, \dots, T$, the normalized likelihood function may be presented as

$$\mathrm{LF}[\mathbf{\Phi}_{N-1}|\mathbf{X}_t] = \mathrm{const}\frac{\det[\mathbf{R}_T]\det\mathbf{T}_N \exp N}{\exp\left[\frac{1}{T}\sum_{t=1}^{T}\mathbf{X}_t^{\mathrm{H}}\mathbf{R}_N^{-1}\mathbf{X}_t\right]}. \tag{53}$$

Since the numerator in (53) does not depend on $\mathbf{\Phi}_{N-1}$, the maximum likelihood estimate $(\widehat{\mathbf{\Phi}}_{N-1})_{\mathrm{ML}}$ should be found by minimizing the denominator in (53):

$$\begin{aligned}\mathbf{x}_t^{\mathrm{H}}\mathbf{R}_N^{-1}\mathbf{x}_t &= \mathbf{x}_t^{\mathrm{H}}\mathrm{diag}(\mathbf{\Phi}_{N-1})\mathbf{T}_N^{(0)-1}\mathrm{diag}^{\mathrm{H}}(\mathbf{\Phi}_{N-1})\mathbf{x}_t \\ &= \mathbf{\Phi}_{N-1}^{\mathrm{T}}\mathrm{diag}(\mathbf{x}_t^{\mathrm{H}})\ \mathbf{T}_N^{(0)-1}\mathrm{diag}(\mathbf{x}_t)\ \mathbf{\Phi}_{N-1}\end{aligned} \tag{54}$$

where $\mathbf{\Phi}_{N-1}^{\mathrm{T}} = [1, e^{i\varphi_1}, \dots, e^{i\varphi_{N-1}}]$ is the vector that needs to be optimized. This means we have to find a constant modulus vector $\mathbf{U}_N$ ($|u_j| = 1$) that minimizes the Hermitian form

$$\mathbf{H} = \frac{1}{T}\sum_{t=1}^{T}\mathrm{diag}(\mathbf{x}_t^{\mathrm{H}})\mathbf{T}_N^{(0)-1}\mathrm{diag}(\mathbf{x}_t)\,. \tag{55}$$

It is clear that the initial solution may be found as the arguments $\widehat{\mathbf{\Phi}}_{\min}$ of the elements of the eigenvector $\mathbf{U}_N$ that corresponds to the minimum eigenvalue of $\mathbf{H}$ (55). The derived solution

$$\widehat{\mathbf{R}}(\widehat{\mathbf{\Phi}}_{\min}) = \mathbf{D}^{\mathrm{H}}\left[\widehat{\mathbf{\Phi}}_{\min}\right]\widehat{\mathbf{R}}_N\mathbf{D}\left[\widehat{\mathbf{\Phi}}_{\min}\right] \tag{56}$$

may then be tested with the sphericity test with the known Toeplitz matrix. If the test does not fit the scenario-free distribution (for the hypothesis H_1), an additional local search in the vicinity of $\widehat{\mathbf{\Phi}}_{\min}$ could be performed. For $T/N \gg 1$, when these initial phase estimates are quite accurate, the search in the vicinity of $\widehat{\mathbf{\Phi}}_{\min}$ may be performed using the linearizations

$$\exp\left(i\left(\varphi_j^o + \Delta_j\right)\right) = \exp\left(i\varphi_j^o\left[1 + i\Delta_j\right]\right). \tag{57}$$

Yet, for a relatively large $T \gg N$, the "minimum" eigenvector $\mathbf{U}_N$ has elements with nearly constant amplitude and a likelihood ratio minimum (for $\mathbf{\Phi}_{N-1}^{\mathrm{H}}\mathbf{\Phi}_{N-1} = 1$) that's very close to

$$\mathrm{MLE} \le \lambda_{\min}^{-1}\left[\frac{1}{T}\sum_{t=1}^{T}\mathrm{diag}(\mathbf{x}_t^{\mathrm{H}})\mathbf{T}_N^{-1}\mathrm{diag}(\mathbf{x}_t)\right] \tag{58}$$

by comparison with $\widehat{\mathbf{R}}(\widehat{\mathbf{\Phi}}_{\min})$ with (58) that allows for this proximity assessment. Therefore, for the model with the a priori known Toeplitz covariance ULA matrix, we got the maximum likelihood estimation (MLE) estimate $(\widehat{\mathbf{\Phi}}_{N-1})_{\mathrm{ML}}$, whose accuracy we may compare against the CRB (48) and use as the benchmark for the ad-hoc estimation techniques, which are derived for the non-ML techniques for this and more complicated scenarios with the fully or partially unknown a priori covariance matrices.

One such ad-hoc technique that could be traced to [4], is the direct exploitation of the Toeplitz covariance matrix properties. Indeed, for the true ($T \to \infty$) covariance matrix $\mathbf{T}_N$ in (49), the following equation exploits the first super-diagonal of the matrix $\mathbf{T}_N$ (with elements $[\mathbf{T}_N]_{p,p+1}$):

$$\begin{aligned}&\mathbf{A}_{N-1}\mathbf{\Phi}_{N-1} + \arg(t_1)\,\mathbf{E}_{N-1} = \arg[\mathbf{R}_N]_{p,p+1} \\ &p = 1, \dots, N-1,\quad \mathbf{E}_{N-1}^{\mathrm{T}} = [1,1,\dots,1],\quad \varphi_o = 0\,.\end{aligned} \tag{59}$$

This equation is accurate and its solution should lead to the true phase errors $\boldsymbol{\varphi}_l, l = 1, \dots, N-1$. Since $\mathbf{A}_{N-1} \in \mathcal{R}^{(N-1)x(N-1)}$,

$$-\mathbf{A}_{N-1} = \begin{bmatrix} -1 & 0 & \dots & & 0 \\ 0 & -1 & 1 & & \\ & & -1 & \ddots & \\ & & & \ddots & \\ 0 & \dots & 0 & -1 & 1 \end{bmatrix} \tag{60}$$

is the invertible matrix and the solution

$$\begin{aligned}\widehat{\mathbf{\Phi}}_{N-1} &= \mathbf{A}_{N-1}^{-1} \\ &\times\left[\arg[\mathbf{R}_N]_{p,p+1} - \arg(t_1)\mathbf{E}_{N-1}\right]\end{aligned} \tag{61}$$

should deliver the unknown accurate phase error values. For the finite sample support T (const), this equation is not accurate and at best, should provide a solution with errors equal to the phase differences between the first super-diagonal elements of the sample matrix (for the no phase calibration errors case). Indeed, simulations conducted for the scenario (23)-(30) demonstrates that phase errors estimated by (61) remain practically the same, with estimation errors of $\varphi_{\max} = 0.001^{\mathrm{o}}$ and $\varphi_{\max} = 180^{\mathrm{o}}$.

Moreover, these errors accurately coincide with the phase differences

$$\arg\left[\widehat{\mathbf{R}}_N\right]_{p,p+1} - \arg[\mathbf{R}_N]_{1,2} \tag{62}$$

of the ideal (no "calibration" errors) sample matrix. It's quite straight-forward to involve other super-diagonals and "average" the sample matrix phase errors, but it is not productive as demonstrated by the results of the simulations introduced below. As follows from TABLE I. , the RMSE of the "calibration" phase errors remains practically the same, irrespective of the number of super-diagonals involved.

TABLE I.

# super-diagonals used	RMSE (deg)
1	12.23
2	10.76
3	11.0

In fact, this is a manifestation of the high correlation of phase fluctuations in the sample matrix [7]. In [5], the authors suggests a technique that somewhat destroys this correlation and improves the estimates. In Part II, we introduce an alternative technique to improve the calibration phase errors estimation accuracy.

At this point, let us investigate the "sphericity" $\mathrm{LR}\left(\widehat{\mathbf{R}}_N^c \middle| \mathbf{T}_N\right)$ (12) and $\mathrm{LR}\left(\widehat{\mathbf{R}}_N^c \middle| \widehat{\mathbf{T}}_N\right)$, where $\widehat{\mathbf{T}}_N$ is the "Gohberg-Semencul" Toeplitz matrix transformation of the sample matrix $\widehat{\mathbf{R}}_N(\widehat{\mathbf{\Phi}}_{N-1})$. One can see that the "corrected" sample matrix $\widehat{\mathbf{R}}_N(\widehat{\mathbf{\Phi}}_{N-1})$ with the RMT-modified eigenvalues, is still reliably identified as a sample matrix of a non-Toeplitz origin. This sensitivity of the LR test is exploited below in our estimation algorithm. It is instructive to compare the efficiency of the MLE algorithm

$$(\widehat{\mathbf{\Phi}}_{N-1})_{\mathbf{ML}} = \arg \mathbf{U}_{\min}\left[\frac{1}{T}\sum_{t=1}^{T} \mathrm{diag}(\mathbf{x}_t^{\mathrm{H}})\mathbf{T}_N^{-1}\mathrm{diag}(\mathbf{x}_t)\right] \tag{63}$$

to the efficiency of the ad-hoc algorithm that we introduced in [13] for the case of the a priori known Toeplitz covariance matrix $\mathbf{T}_N$. We propose to estimate the arguments of the elements of the "maximum" eigenvector $\mathbf{U}_{\max}$ of the element-wise matrix ratio Δ_N:

$$\mathbf{\Delta}_N = \frac{\widehat{\mathbf{R}}_N}{\mathbf{T}_N}. \tag{64}$$

For $\widehat{\mathbf{R}}_N \to \mathbf{R}_N$ $(T \to \infty)$,

$$\begin{gathered}\mathbf{\Delta}_N \to \mathrm{diag}(\mathbf{\Phi}_{N-1})\mathbf{1}_N\mathbf{1}_N^{\mathrm{T}}\mathrm{diag}^{\mathrm{H}}(\mathbf{\Phi}_{N-1}),\\ \mathbf{1}_N^{\mathrm{T}} = [1,1,\dots,1]\,.\end{gathered} \tag{65}$$

The performance degradation of the technique

$$\widehat{\mathbf{\Phi}}_{N-1} = \arg \mathbf{U}_{\max}\left[\frac{\widehat{\mathbf{R}}_N}{\mathbf{T}_N}\right] \tag{66}$$

with respect to the ML estimate (63) and the CRB (48) provides an important insight into the relative efficiency of these techniques. Simulation results introduced in TABLE II. demonstrate the essential superiority of the ML algorithm (63).

TABLE II.

MLE Alg (63) **Phase errors: Sqrt 2nd moment (deg)**		**N=17**		**N=100**	
		φ_{max}		φ_{max}	
		5^o	180^o	5^o	180^o
T	**100**	2.19	2.19	2.88	2.88
	300	1.25	1.25	1.65	1.65
	3E3	0.38	0.38	0.55	0.55
	3E4	0.13	0.13	0.17	0.17

IV. "Blind" Calibration of the ULA Arrays Operating in the "Oversampled" Regime

As discussed in Introduction, receive ULA arrays of the HF OTH radars operate in the "oversampled" regime most of the time with $d/\lambda < 1/2$. Correspondingly, there is always the "invisible" sector in μ:

$$\frac{2\pi d}{\lambda} < |\mu| \le \pi\,. \tag{67}$$

If the antenna is properly calibrated, very little power "leaks" from the visible sector into the invisible one via the beampattern sidelobes. Therefore, by finding the estimates of the calibration phase errors that minimize the total power within the "invisible" sector, we may somewhat calibrate our ULA. This idea was proposed in our paper [6], where a quite efficient phase errors compensation was demonstrated for a symmetric spatial power spectrum steered into the orthogonal to linear array direction. Due to the conference format paper in [6], a number of important issues have not been explored in detail.

In particular, for an asymmetric spatial spectrum one may expect a non-trivial phase-only solution that minimizes the "invisible" sector power, even for a properly calibrated antenna array. Indeed, if the spectrum is symmetric but shifted in some non-zero direction, one may expect that the optimal phase distribution should at least "move" this spectrum to the center of the visible arc. Obviously the ideal linear phase progression is irrelevant, but whether the optimum phase solution is ideally linear in the general case needs to be verified. Therefore we first have to explore the optimum phase solutions that minimize the "invisible" power for properly calibrated arrays, and then check that in the presence of "calibration" phase errors the optimal solution is the sum of these "calibration" phase errors and the solution for an ideally calibrated array. Let us provide the analytical description of this optimization routine.

For the given set of training data $\mathbf{Y}_t, t = 1,\dots,T$,

$$\mathbf{Y}_t = \mathrm{diag}[\mathbf{\Phi}_{N-1}]\mathbf{X}_t,\ \ \mathbf{X}_t = \mathbf{T}_N^{\frac{1}{2}}\boldsymbol{\xi}_t,\ \ \boldsymbol{\xi}_t \sim \mathbb{C}\mathcal{N}(0,\mathbf{I}_N)\,, \tag{68}$$

the power stored in the "invisible" sector may be presented as the limit

$$\sigma_{\text{inv}}^2 = \lim_{N\to\infty}\frac{1}{N}\sum_{t=1}^{T}\mathbf{X}_t^{\text{H}}\sum_{j=1}^{N}\mathbf{S}(\boldsymbol{\mu}_j)\mathbf{S}^{\text{H}}(\boldsymbol{\mu}_j)\mathbf{X}_t\,, \tag{69}$$

Since

$$\begin{aligned}\mathbf{R}_{\text{inv}} &= \lim_{N\to\infty}\frac{1}{N}\sum_{j=1}^{N}\mathbf{S}(\boldsymbol{\mu}_j)\mathbf{S}^{\text{H}}(\boldsymbol{\mu}_j)\Rightarrow\\ &\boldsymbol{\mu}_{j+1}-\boldsymbol{\mu}_j\to 0\\ &\Rightarrow 2\int_{2\pi d/\lambda}^{\pi}\cos[\mu(n-k)]d\mu\\ &= C\left[\mathbf{I}_N-\frac{\sin\left(\frac{2\pi d}{\lambda}(n-k)\right)}{\pi(n-k)}\right]\end{aligned} \tag{70}$$

which for $d/\lambda\to 1/2, \mathbf{R}_{\text{inv}}\to 0$. The covariance matrix of the "visible" sector $\mathbf{R}_{\text{vis}}$ may be found by integration over θ within the limits

$$|\mu|<\frac{2\pi d}{\lambda}\sin\theta,\quad |\theta|\le\frac{\pi}{2}. \tag{71}$$

For antenna elements with an ideal beampattern, we have

$$\mathbf{R}_{\text{vis}} = \frac{\lambda}{2\pi d}\int_{-\pi/2}^{\pi/2}\exp i\left[\frac{2\pi d}{\lambda}(m-n)\sin\theta\right]d\theta\,, \tag{72}$$

while for the antenna element beampattern approximated by the function $\cos\theta$, we have

$$\begin{aligned}\mathbf{R}_{\text{vis}} &= \frac{\lambda}{2\pi d}\int_{-1}^{1}\cos\left[\left(\frac{2\pi d}{\lambda}x\right)(m-n)\right]dx\\ &= \frac{\lambda}{2d}\frac{\sin\frac{2\pi d}{\lambda}(n-k)}{\pi(n-k)}.\end{aligned} \tag{73}$$

The un-normalized covariance matrices $\mathbf{R}_{\text{inv}}$ and $\mathbf{R}_{\text{vis}}$ are therefore defined as

$$\mathbf{R}_{\text{inv}} = \left[\mathbf{I}-\frac{\sin\frac{2\pi d}{\lambda}(n-k)}{\pi(n-k)}\right],\quad n,k=1,\dots,N \tag{74}$$

with power

$$\sigma_{\text{inv}}^2 = \left[\frac{1}{1-2d/\lambda}\right]^{-1}, \tag{75}$$

and

$$\mathbf{R}_{vis} = \left[\frac{\sin\frac{2\pi d}{\lambda}(n-k)}{\pi(n-k)}\right]^{-1} \tag{76}$$

with power

$$\sigma_{\text{vis}}^2 = \left[\frac{\lambda}{2d}\right]^{-1} \tag{77}$$

for

$$\frac{d}{\lambda}\to\frac{1}{2},\quad \sigma_{\text{inv}}^2\to 0,\quad \sigma_{\text{vis}}^2\to 1\,. \tag{78}$$

Since

$$\mathbf{R}_{\text{inv}}+\mathbf{R}_{\text{vis}} = \mathbf{I}_N\,, \tag{79}$$

it is clear that the minimization of the power stored in the "invisible" sector is equivalent to the maximization of the ratio for the power collected from the "visible" sector to the power "stored" in the "invisible" one. Note that if we consider the ideal antenna element's beampattern $(f_{el}(\theta)=1)$, we get the "visible" sector covariance matrix

$$\begin{aligned}\mathbf{R}_{\text{vis}} &= \frac{1}{\pi}\int_{-\pi}^{\pi}\exp\left\{i\left[\frac{2\pi d}{\lambda}(n-k)\sin\theta\right]\right\}d\theta\\ &= \Im_o\left[\frac{2\pi d}{\lambda}(n-k)\right]\end{aligned} \tag{80}$$

where $\Im_o(x)$ is the Bessel function [17]. Yet, if we assume the beampattern of the single antenna element $f(\theta)$ to be

$$f(\theta)=\cos\theta\,,\qquad -\frac{\pi}{2}<\theta<\frac{\pi}{2} \tag{81}$$

we get the same expression as (76), (77). Assuming $d/\lambda<0.5$, let us minimize the power σ_{inv}^2

$$\sigma_{\text{inv}}^2 = \frac{1}{T}\sum_{t=1}^{T}\mathbf{Y}_t^{\text{H}}\text{diag}[e^{i\boldsymbol{\psi}_{N-1}}]\mathbf{R}_{\text{inv}}\text{diag}[e^{-i\boldsymbol{\psi}_{N-1}}]\,\mathbf{Y}_t \tag{82}$$

by optimization of the phases $\boldsymbol{\psi}_j, j=2,\dots,N-1$ in

$$\text{diag}[e^{i\boldsymbol{\psi}_{N-1}}] = \begin{bmatrix}1 & & & 0\\ & e^{i\psi_1} & & \\ & & \ddots & \\ 0 & & & e^{i\psi_{N-1}}\end{bmatrix}. \tag{83}$$

Since

$$\mathbf{Y}_t^{\text{H}}\text{diag}[e^{i\boldsymbol{\psi}_{N-1}}] = \mathbf{E}^{\text{H}}[e^{-i\boldsymbol{\psi}_{N-1}}]\text{diag}[\mathbf{Y}_t^{\text{H}}] \tag{84}$$

we get

$$\sigma_{\text{inv}}^2 = \frac{1}{T}\mathbf{E}^{\text{H}}(\boldsymbol{\psi}_{N-1}) \times \sum_{t=1}^{T} \text{diag}[\mathbf{Y}_t^{\text{H}}]\mathbf{R}_{\text{inv}}\text{diag}[\mathbf{Y}_t]\,\mathbf{E}(\boldsymbol{\psi}_{N-1}) , \tag{85}$$

where

$$\mathbf{E}^{\text{H}}(\boldsymbol{\psi}_{N-1}) = \begin{bmatrix} 1 \\ e^{-i\psi_1} \\ \vdots \\ e^{-i\psi_{N-1}} \end{bmatrix}^{\text{T}} . \tag{86}$$

Therefore, we have the non-linear optimization problem:

$$\text{Find min}\, \mathbf{E}^{\text{H}}(\boldsymbol{\psi}_{N-1})\mathbf{B}\,\mathbf{E}(\boldsymbol{\psi}_{N-1}) \tag{87}$$

where

$$\mathbf{B} = \frac{1}{T}\sum_{t=1}^{T} \text{diag}^{\text{H}}[\mathbf{Y}_t]\mathbf{R}_{\text{inv}}\text{diag}[\mathbf{Y}_t] . \tag{88}$$

As discussed above, we consider the following:

Case 1 No phase "calibration" errors:

$$\mathbf{Y}_t = \mathbf{X}_t = \mathbf{T}_N^{\frac{1}{2}}\boldsymbol{\xi}_t, \quad \boldsymbol{\xi}_t \sim \mathbb{C}\mathcal{N}(0, \mathbf{I}_N) \tag{89}$$

Case 2 Phase "calibration" errors present:

$$\mathbf{Y}_t = \text{diag}[\boldsymbol{\Phi}_{N-1}]\mathbf{X}_t, \;\; \mathbf{X}_t = \mathbf{T}_N^{\frac{1}{2}}\boldsymbol{\xi}_t, \quad \boldsymbol{\xi}_t \sim \mathbb{C}\mathcal{N}(0, \mathbf{I}_N) . \tag{90}$$

Since

$$\begin{aligned} \min_{\psi}[\mathbf{E}^{\text{H}}(\boldsymbol{\psi}_{N-1})\mathbf{B}\,\mathbf{E}(\boldsymbol{\psi}_{N-1})] & \\ = \max \frac{\mathbf{E}^{\text{H}}(\boldsymbol{\psi}_{N-1})\mathbf{I}_{\text{N}}\mathbf{E}(\boldsymbol{\psi}_{N-1})}{\mathbf{E}^{\text{H}}(\boldsymbol{\psi}_{N-1})\mathbf{B}\,\mathbf{E}(\boldsymbol{\psi}_{N-1})} & \\ \equiv q(\boldsymbol{\psi}_N) , & \end{aligned} \tag{91}$$

we may use the steepest descent algorithm from [18]:

$$\boldsymbol{\psi}_N^{t+1} = \boldsymbol{\psi}_N^t + \alpha_t \nabla\left(q\left(\boldsymbol{\psi}_N^{(t)}\right)\right) \tag{92}$$

where

$$\nabla\left(q\left(\boldsymbol{\psi}_N^{(t)}\right)\right) = \begin{bmatrix} \frac{\partial q\left(\boldsymbol{\psi}_N^{(t)}\right)}{\partial \psi_1} \\ \vdots \\ \frac{\partial q\left(\boldsymbol{\psi}_N^{(t)}\right)}{\partial \psi_N} \end{bmatrix} \tag{93}$$

$$\frac{\partial \mathbf{E}^{\text{H}}(\boldsymbol{\psi}_N)}{\partial \boldsymbol{\psi}_k} = [0, \ldots, 0, -i\exp(-i\boldsymbol{\psi}_k), 0, \ldots, 0] = \text{i}\,\mathbf{E}_{\text{k}}^{\text{H}} . \tag{94}$$

With respect to (94) we get [18]:

$$\frac{\partial q}{\partial \boldsymbol{\psi}_k} = -\frac{2\,\text{Im}\left\{\mathbf{E}_{\text{k}}^{\text{H}}\left(\mathbf{I} - q\left(\boldsymbol{\psi}_N^{(t)}\right)\mathbf{B}\right)\mathbf{E}\left(\boldsymbol{\psi}_N^{(t)}\right)\right\}}{\mathbf{E}^{\text{H}}\left(\boldsymbol{\psi}_N^{(t)}\right)\mathbf{B}\,\mathbf{E}\left(\boldsymbol{\psi}_N^{(t)}\right)} . \tag{95}$$

The scalar α_t in (95) should be searched for at each iteration to achieve the maximum $q\left(\boldsymbol{\psi}_N^{(t)}\right)$ within the first-order expansion for $\psi_N^{(t+1)}$

$$\begin{aligned} \boldsymbol{\psi}_N^{t+1} &= \boldsymbol{\psi}_N + \alpha_t\left[\nabla q\left(\boldsymbol{\psi}_N^{(t)}\right)\right] \\ &= \exp\left(\boldsymbol{\psi}_N^{(t)}\right)\left(\mathbf{I} + i\alpha_t\left(\nabla q\left(\boldsymbol{\psi}_N^{(t)}\right)\right)\right) . \end{aligned} \tag{96}$$

This result is quite general and by the replacement in (95), $\mathbf{I}_N \Rightarrow \mathbf{F}_N$ could be used for maximization of the ratio of the two Hermitian forms

$$\mathbf{P} = \frac{\mathbf{E}^{\text{H}}(\boldsymbol{\psi}_N)\mathbf{F}_{\text{N}}\mathbf{E}(\boldsymbol{\psi}_N)}{\mathbf{E}^{\text{H}}(\boldsymbol{\psi}_N)\mathbf{B}\,\mathbf{E}(\boldsymbol{\psi}_N)} . \tag{97}$$

Analysis of the Monte-Carlo simulations results are introduced in the next section.

First let us specify the optimization function for $T \to \infty$ that may be used as the benchmark for $T < \infty$. Let us consider

$$\begin{aligned} \lim_{T\to\infty}\frac{1}{T}\sum_{t=1}^{T}\text{diag}^{\text{H}}[\mathbf{Y}_t]\mathbf{R}_{\text{inv}}\text{diag}[\mathbf{Y}_t] = & \\ \text{diag}^{\text{T}}[\boldsymbol{\Phi}_{N-1}]\frac{1}{T}\sum_{t=1}^{T}\text{diag}^{\text{H}}\left[\mathbf{T}_N^{\frac{1}{2}}\boldsymbol{\xi}_t\right]\mathbf{R}_{\text{inv}}\text{diag}\left[\mathbf{T}_N^{\frac{1}{2}}\boldsymbol{\xi}_t\right] & \\ \times \text{diag}[\boldsymbol{\Phi}_{N-1}] . & \end{aligned} \tag{98}$$

Let

$$\mathbf{T}_N^{\frac{1}{2}}\boldsymbol{\xi}_t = \sum_{k=1}^{N}\left(\mathbf{T}_N^{\frac{1}{2}}\mathbf{e}_k\right)\boldsymbol{\xi}_{tk} \tag{99}$$

where $\mathbf{e}_k$ is the N-variate column vector with ones in the k-th position and zeros in all the other entries. Then

$$\begin{aligned} \text{diag}^{\text{H}}[\mathbf{X}_t]\mathbf{R}_{\text{inv}}\text{diag}[\mathbf{X}_t] = & \\ \sum_{k=1}^{N}\sum_{l=1}^{N}\boldsymbol{\xi}_{kl}^*\text{diag}^{\text{H}}\left[\mathbf{T}_N^{\frac{1}{2}}\mathbf{e}_k\right]\mathbf{R}_{\text{inv}}\text{diag}\left[\mathbf{T}_N^{\frac{1}{2}}\mathbf{e}_l\right]\boldsymbol{\xi}_{kl} . & \end{aligned} \tag{100}$$

Since

$$\lim_{T\to\infty}\frac{1}{T}\sum_{t=1}^{T}\boldsymbol{\xi}_{lk}^*\boldsymbol{\xi}_{lk} = \begin{cases} \sigma^2 \text{ for } k = l, \\ 0 \text{ for } k \neq l, \end{cases} \quad (\sigma^2 = 1) \tag{101}$$

we have

$$\lim_{T\to\infty}\frac{1}{T}\sum_{t=1}^{T}\mathrm{diag}^{\mathrm{H}}[\mathbf{X}_t]\mathbf{R}_{\mathrm{inv}}\mathrm{diag}[\mathbf{X}_t] = \sigma^2\sum_{k=1}^{N}\mathrm{diag}^{\mathrm{H}}\left[\mathbf{T}_N^{\frac{1}{2}}\mathbf{e}_k\right]\mathbf{R}_{\mathrm{inv}}\mathrm{diag}\left[\mathbf{T}_N^{\frac{1}{2}}\mathbf{e}_k\right] \quad (102)$$

and the optimization function is

$$\lim_{T\to\infty}\mathbf{P}_T = \sigma^2\mathbf{E}^{\mathrm{H}}(\boldsymbol{\psi}_{N-1}) \times\left[\sum_{k=1}^{N}\mathrm{diag}^{\mathrm{H}}\left[\mathrm{D}[\boldsymbol{\psi}_{N-1}]\mathbf{T}_N^{\frac{1}{2}}\mathbf{e}_k\right]\mathbf{R}_{\mathrm{inv}}\right] \times\mathrm{diag}[\mathbf{E}(\boldsymbol{\psi}_{N-1})]\,. \quad (103)$$

Note that for the "invisible" power in the calibrated array with no phase optimization, when $\mathbf{E}^{\mathrm{H}}(\boldsymbol{\psi}_{N-1}) = [1,1,\ldots,1]$, we get

$$\mathbf{P}_{\mathrm{inv}} = \sigma^2\mathrm{Tr}[\mathbf{T}_N\mathbf{R}_{\mathrm{inv}}]\,. \quad (104)$$

Note that for the symmetric matrix $\mathbf{T}_N$, we should expect the real-valued optimum solution if no "calibration" phase errors are present.

V. Simulation Results

In this section we start from the "benchmark" CRB (48) and compare these predictions with the results of the Monte-Carlo simulations of the ML "calibration" phase errors estimation algorithm (55)-(58) developed for the a priori known covariance matrix. Both CRB analysis and ML "calibration" phase estimation are conducted for the a priori known covariance matrix of the impinging signal on an ideally calibrated ULA signal, and therefore serve as the "benchmark" for comparison with the more practical algorithms. In particular, we are going to compare the "benchmark" performance with the following:

- "Invariant" algorithm with the true $\arg t_1$:

$$\widehat{\boldsymbol{\Phi}}_{N-1} = (\mathbf{A}_{N-1}^{\mathrm{H}}\mathbf{A}_{N-1})^{\mathrm{H}}\mathbf{A}_{N-1}^{\mathrm{H}} \times\left[\arg\left[\widehat{\mathbf{R}}_N\right]_{p,p+1} - \arg(t_1)\mathbf{E}_{N-1}\right] \quad (105)$$

- "Invariant" algorithm in (105) but with the estimated $\arg\hat{t}_1$ in place of $\arg t_1$, where

$$[\arg\hat{t}_1] = \frac{1}{N-1}\sum_{p=1}^{N-1} r_{p,p+1} \quad (106)$$

- "Invariant" estimation algorithm for ULA arrays operating in the over-sampled regime with $d/\lambda < 0.5$ for different $d/\lambda = 0.2, 0.3, 0.4$.
- Ad-hoc algorithm for the a priori known Toeplitz covariance matrix, proposed in [13]

First, let us compare the CRB predictions (48) with the ML algorithm (55). Specifically, we will analyze the argument (phases) of the eigenvector $\mathbf{U}_{\min}$ that corresponds to the minimal eigenvalue of the Hermitian matrix $\mathbf{H}$ in (55). Comparison of the minimal and maximal phase estimation errors over the array aperture, predicted by the CRB (48) and averaged over 1000 trials, demonstrated rather good correspondence between the CRB predictions and simulation results. In fact, the maximal phase errors are predicted a bit more accurately by the CRB, while the minimal errors are slightly underestimated by the CRB. Recall that positions of the maximal and the minimal phase estimation errors over the aperture correspond to the diagonal elements of the inverted covariance matrix with the maximum and minimum values correspondingly.

Overall, in Fig. 16-Fig. 31 we observe quite good correspondence between the CRB predictions and ML simulation results for the tested scenarios with the sample volume T, significantly exceeding the matrix dimension N ($T >> N$).

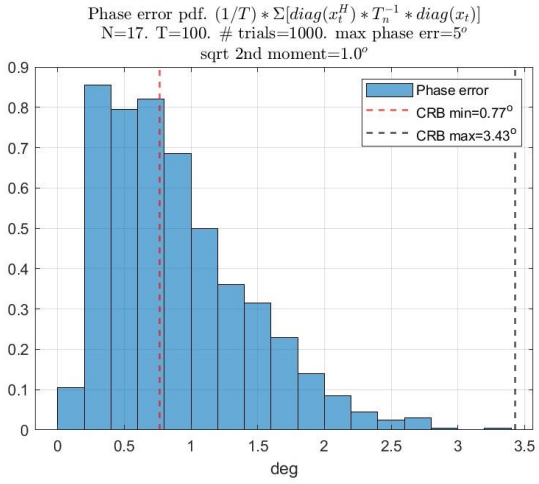

Fig. 16. Phase error PDF of ML alg. (55) with CRB. N=17, T=100, max phase error = 5°

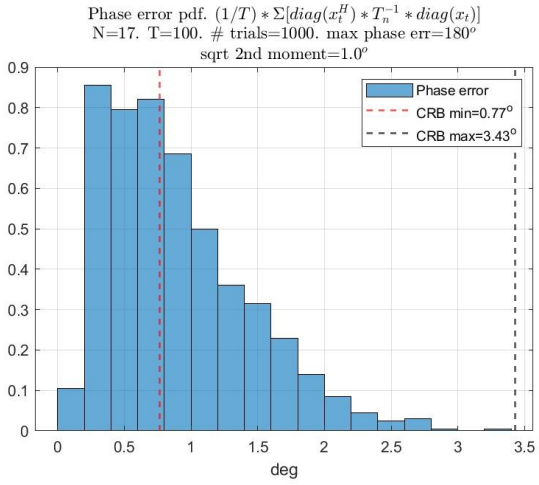

Fig. 17 Phase error PDF of ML alg. (55) with CRB. N=17, T=100, max phase error = 180°

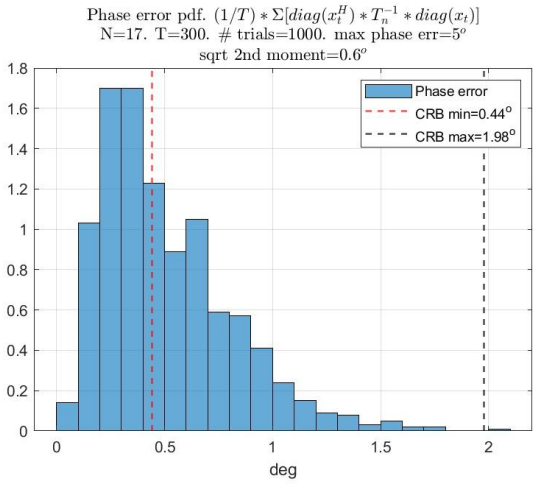

Fig. 18. Phase error PDF of ML alg. (55) with CRB. N=17, T=300, max phase error = 5°

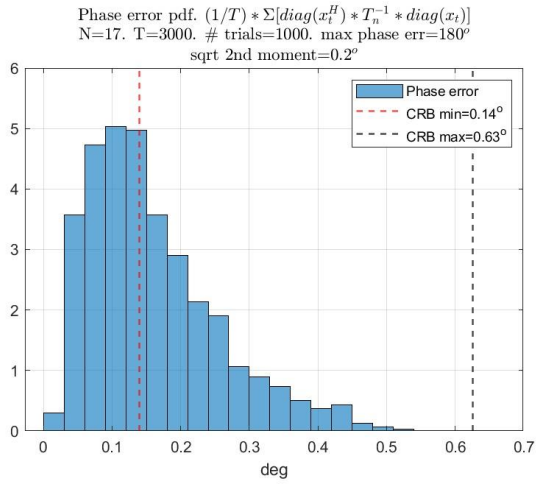

Fig. 21. Phase error PDF of ML alg. (55) with CRB. N=17, T=3000, max phase error = 180°

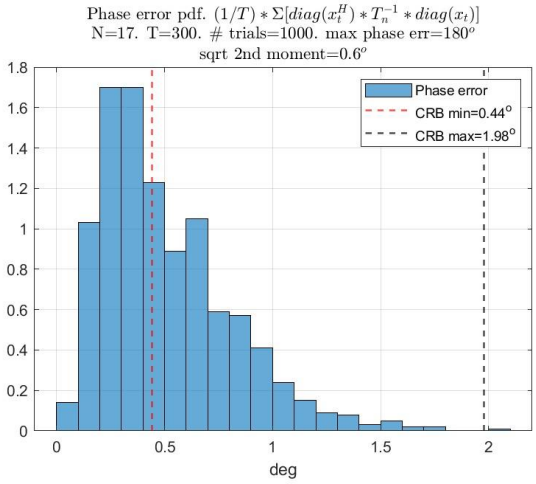

Fig. 19. Phase error PDF of ML alg. (55) with CRB. N=17, T=300, max phase error = 180°

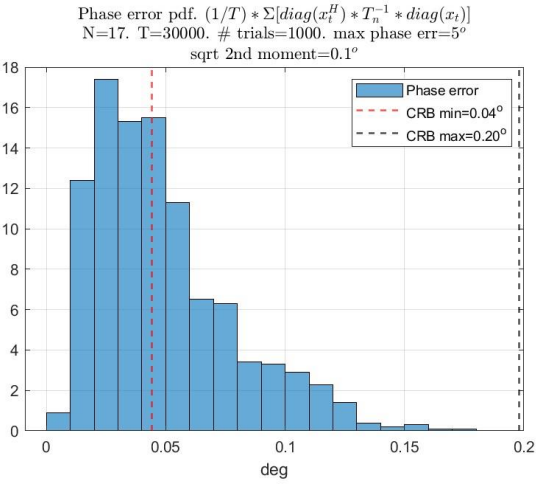

Fig. 22. Phase error PDF of ML alg. (55) with CRB. N=17, T=30000, max phase error = 5°

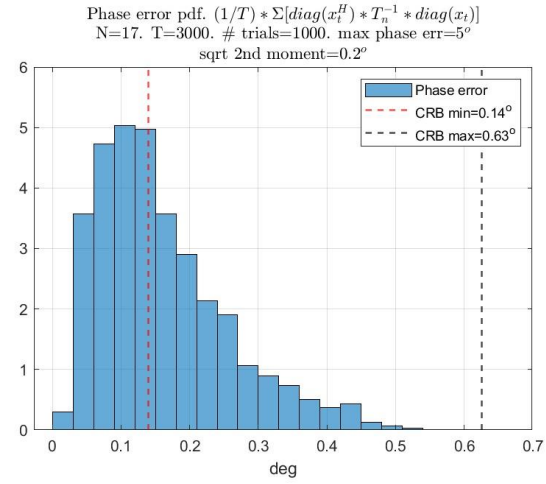

Fig. 20. Phase error PDF of ML alg. (55) with CRB. N=17, T=3000, max phase error = 5°

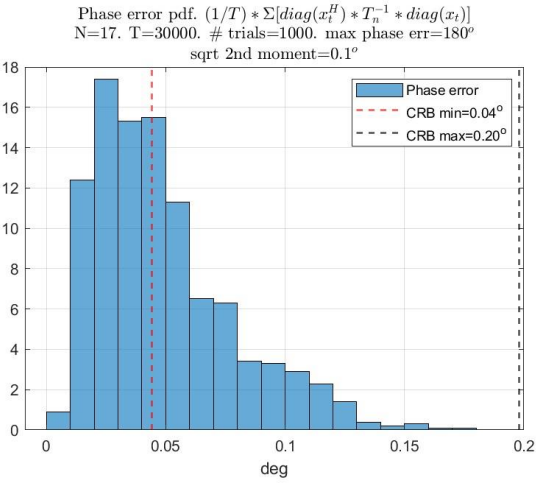

Fig. 23. Phase error PDF of ML alg. (55) with CRB. N=17, T=30000, max phase error = 180°

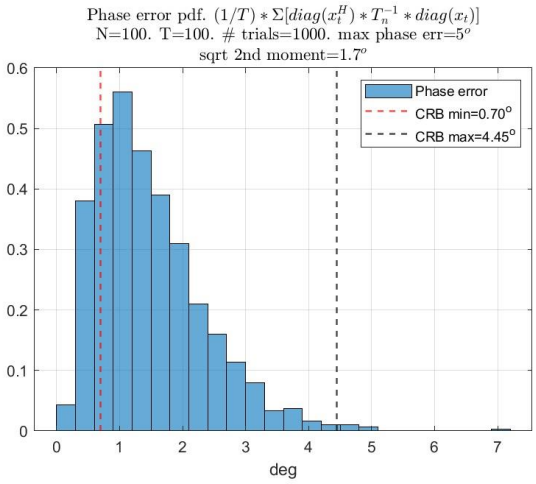

Fig. 24. Phase error PDF of ML alg. (55) with CRB. N=100, T=100, max phase error = 5°

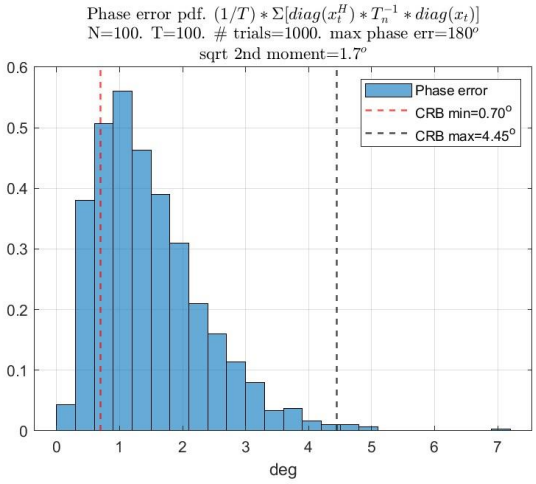

Fig. 25. Phase error PDF of ML alg. (55) with CRB. N=100, T=100, max phase error = 180°

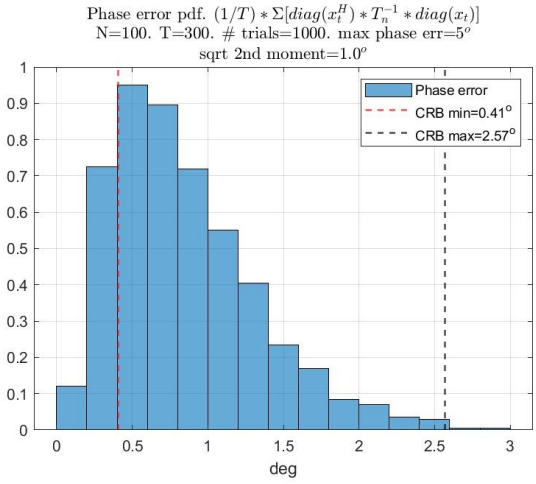

Fig. 26. Phase error PDF of ML alg. (55) with CRB. N=100, T=300, max phase error = 5°

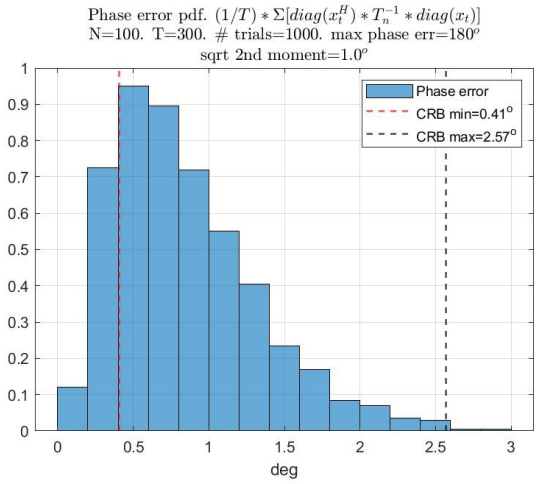

Fig. 27. Phase error PDF of ML alg. (55) with CRB. N=100, T=300, max phase error = 180°

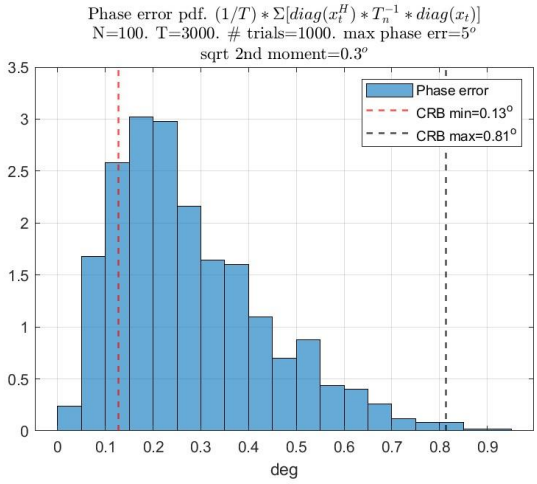

Fig. 28. Phase error PDF of ML alg. (55) with CRB. N=100, T=3000, max phase error = 5°

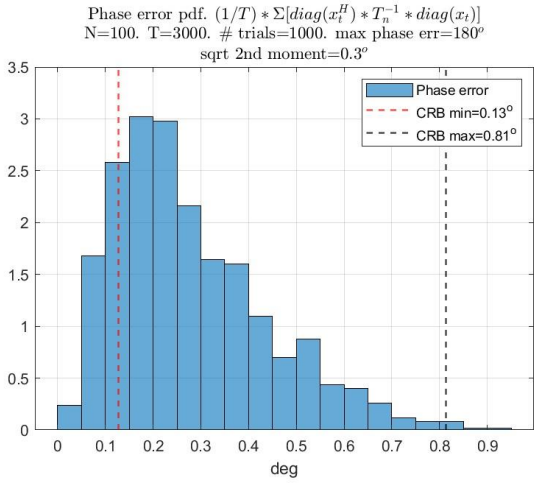

Fig. 29. Phase error PDF of ML alg. (55) with CRB. N=100, T=3000, max phase error = 180°

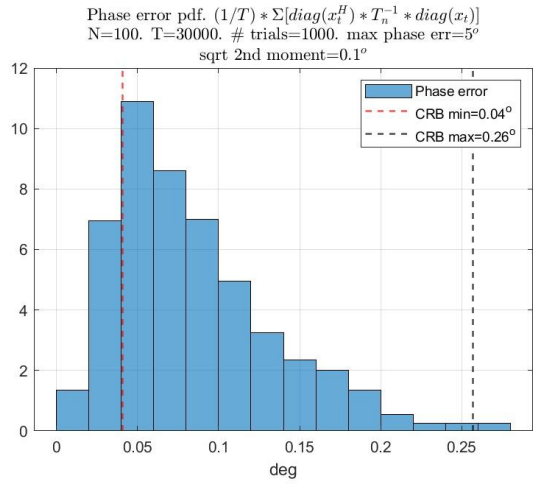

Fig. 30. Phase error PDF of ML alg. (55) with CRB. N=100, T=30000, max phase error = 5°

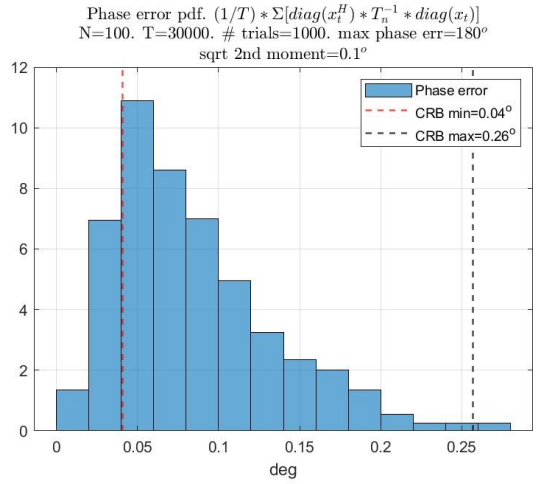

Fig. 31. Phase error PDF of ML alg. (55) with CRB. N=100, T=30000, max phase error = 180°

These results also suggest that for $T >> N$, the phases of the "minimal" eigenvector are very close to the optimum and further solution specification may not be needed. The most important observation is about the "argumental" type of convergence to the true phase values that require an asymptotically large sample volume T for small estimation errors. The eigenspectrum of the covariance matrix plays a certain role since it defines the $\mathbf{R}_{nn}^{-1}/\mathbf{R}_{nn}$ ratio, but in any case the sample volume T should significantly exceed the array dimension N for accurate enough phase estimation errors to be achieved. Compare this property with the DOA estimation of m strong signals, when $T \geq m$ is the sufficient sample support for the accurate enough DOA estimation (under high SNR conditions). This comparison illustrates the most striking distinction between strong and weak convergence [14].

Let us now analyze the efficiency of the "invariant" technique (105), with the accurate value of the first super-diagonal $\arg(t_1)$ of the matrix $\mathbf{T}_N$. Since the true covariance lag is used here, we may treat this algorithm as a simplified version of the algorithm for the a priori known covariance matrix. Yet, as follows from the Fig. 32-Fig. 47 data, the square root of the 2nd moment of the estimated phase increases by almost 5 dB.

TABLE III.

"Invariant" ML Alg (105). Phase errors: Sqrt 2nd moment (deg). Linear shift removed		N=17		N=100	
		φ_{max}		φ_{max}	
		5^o	180^o	5^o	180^o
T	**100**	9.5	9.5	29.9	29.9
	300	5.5	5.5	16.9	16.9
	3E3	1.8	1.8	5.3	5.3
	3E4	0.5	0.5	1.7	1.7

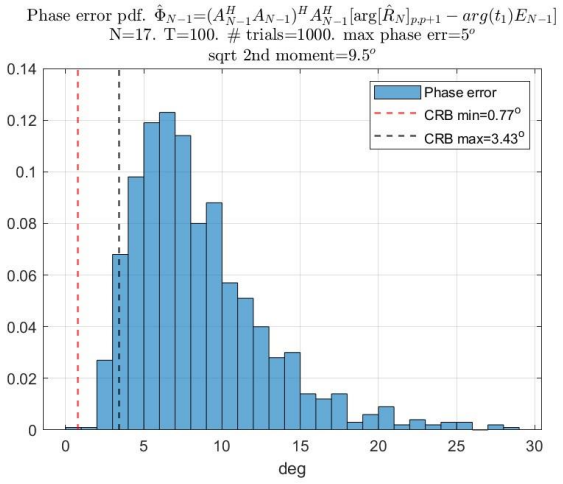

Fig. 32. Phase error PDF of "invariant" alg. (105) with CRB. N=17, T=100, max phase error = 5°

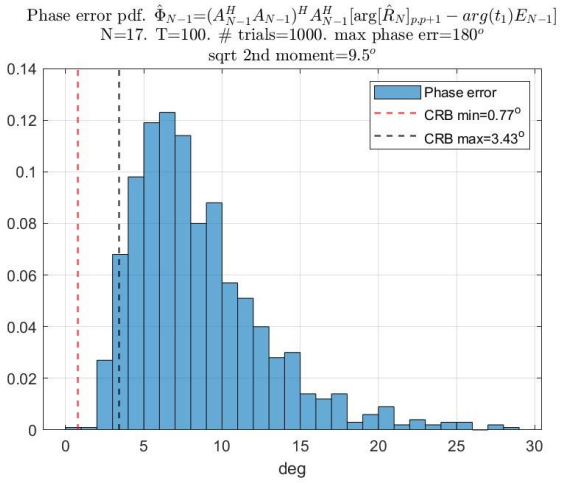

Fig. 33. . Phase error PDF of "invariant" alg. (105) with CRB. N=17, T=100, max phase error = 180°

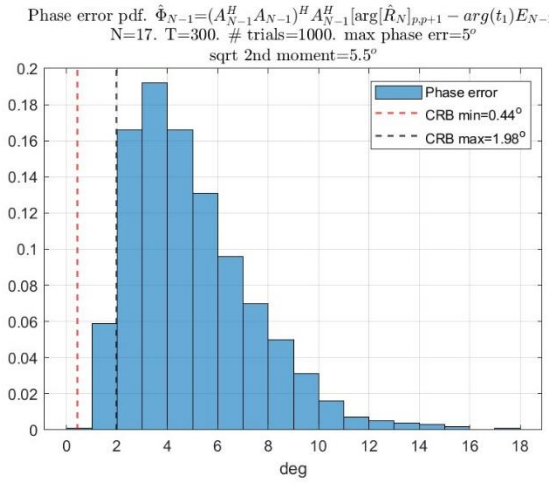

Fig. 34. . Phase error PDF of "invariant" alg. (105) with CRB. N=17, T=300, max phase error = 5°

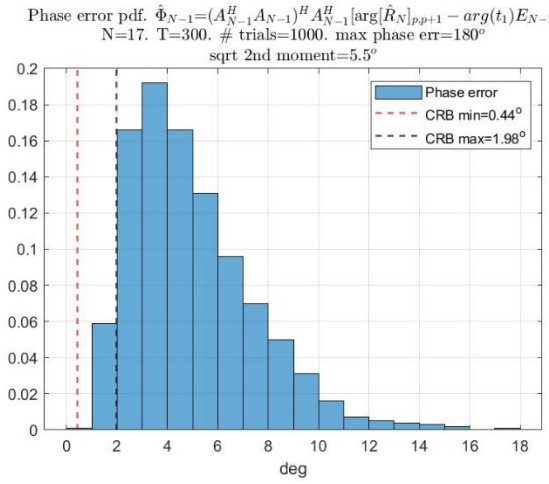

Fig. 35. Phase error PDF of "invariant" alg. (105) with CRB. N=17, T=300, max phase error = 180°

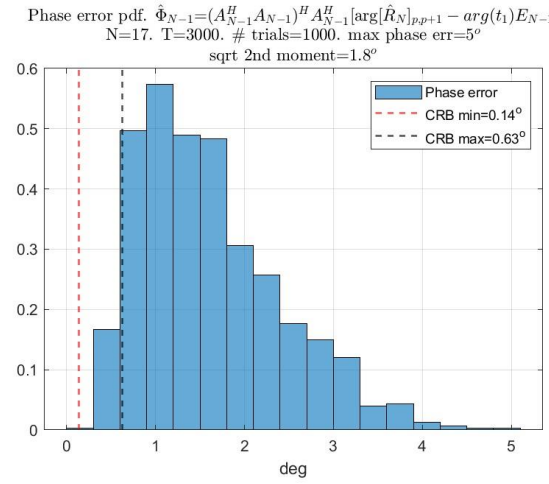

Fig. 36. Phase error PDF of "invariant" alg. (105) with CRB. N=17, T=3000, max phase error = 5°

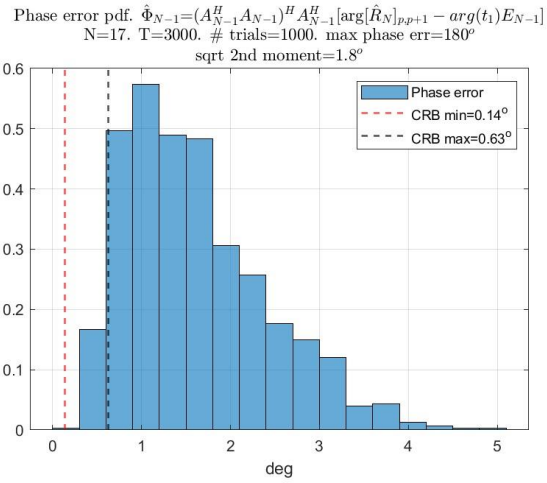

Fig. 37. Phase error PDF of "invariant" alg. (105) with CRB. N=17, T=3000, max phase error = 180°

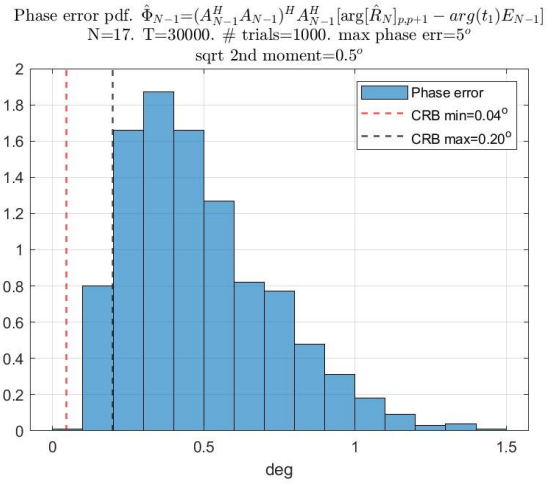

Fig. 38. Phase error PDF of "invariant" alg. (105) with CRB. N=17, T=30000, max phase error = 5°

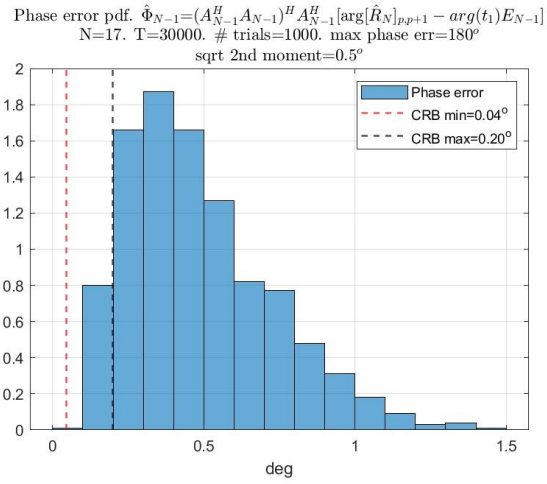

Fig. 39. Phase error PDF of "invariant" alg. (105) with CRB. N=17, T=30000, max phase error = 180°

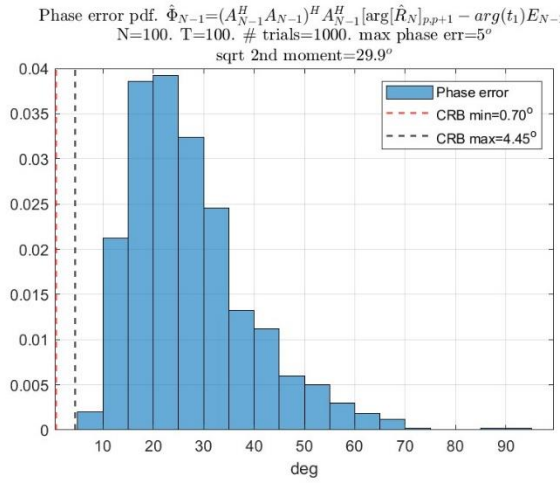

Fig. 40. Phase error PDF of "invariant" alg. (105) with CRB. N=100, T=100, max phase error = 5°

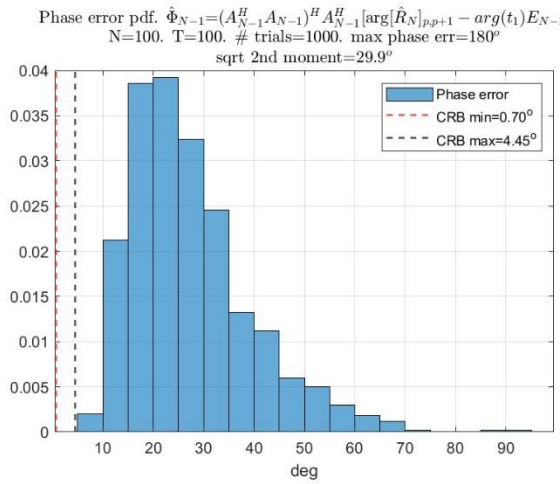

Fig. 41. Phase error PDF of "invariant" alg. (105) with CRB. N=100, T=100, max phase error = 180°

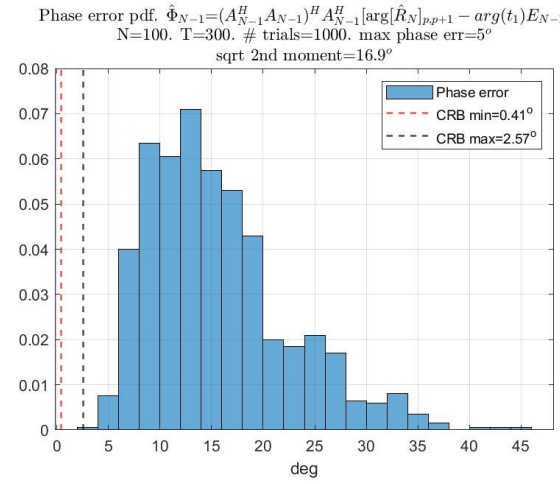

Fig. 42. . Phase error PDF of "invariant" alg. (105) with CRB. N=100, T=300, max phase error = 5°

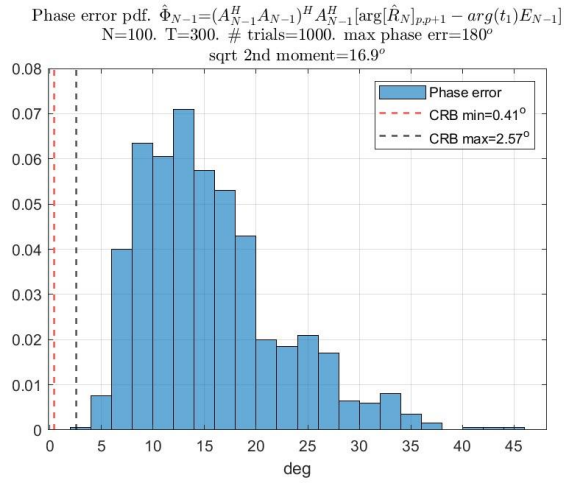

Fig. 43. Phase error PDF of "invariant" alg. (105) with CRB. N=100, T=300, max phase error = 5°

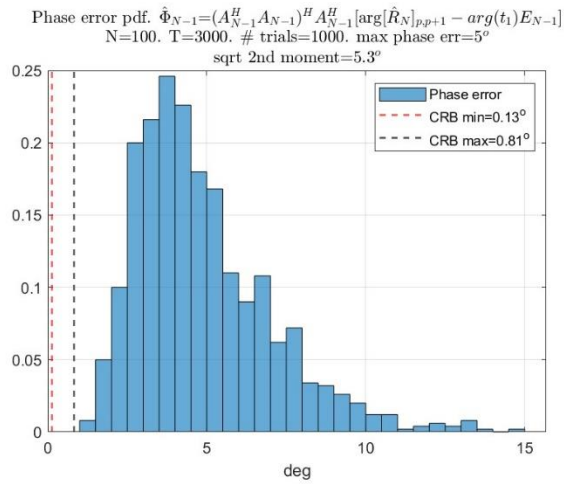

Fig. 44. Phase error PDF of "invariant" alg. (105) with CRB. N=100, T=3000, max phase error = 5°

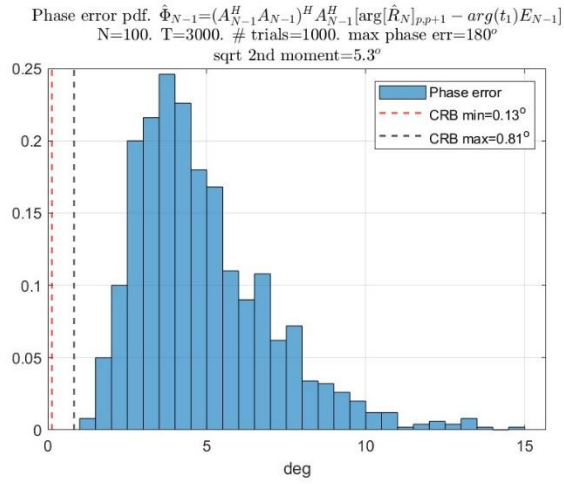

Fig. 45. Phase error PDF of "invariant" alg. (105) with CRB. N=100, T=3000, max phase error = 180°

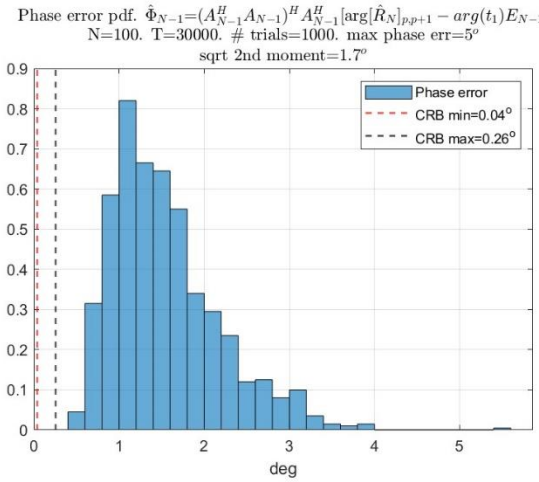

Fig. 46. Phase error PDF of "invariant" alg. (105) with CRB. N=100, T=30000, max phase error = 5°

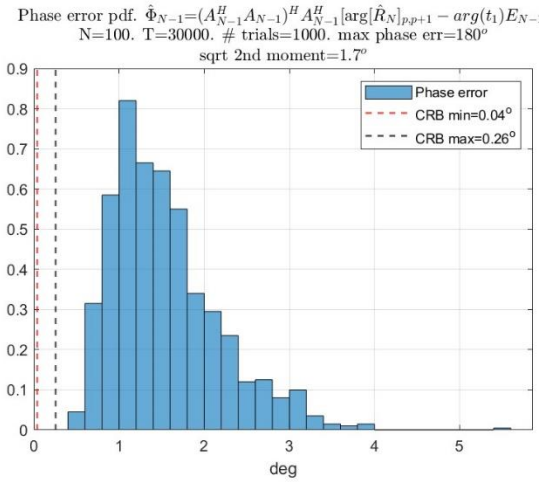

Fig. 47. Phase error PDF of "invariant" alg. (105) with CRB. N=100, T=30000, max phase error = 180°

It is most interesting that the phase estimation errors in this technique do not depend on the dynamic range of the calibration phase errors. Indeed, for $|\varphi_{\max}| = 5^{\circ}$ and $|\varphi_{\max}| = 180^{\circ}$ the estimation errors remain practically identical (see TABLE III.). What is also important is that when $\arg(\hat{t}_1)$, the average over the first super-diagonal elements, is used instead of the true argument $\arg(t_1)$, for $T \geq 100$ and N = 100 our phase estimation accuracy remains practically the same as compared to the ideal $\arg(t_1)$. For N = 17 with much smaller number of averaging elements for $\arg(\hat{t}_1)$ estimation, the "calibration" phase estimation accuracy only marginally degraded.

Practical independence of the estimation accuracy in the method (106) on the dynamic range of the "calibration" phase errors has an obvious explanation. Indeed, in the method (106) we associate the arguments (phases) of the sample matrix super-diagonal elements $\arg\left[\widehat{\mathbf{R}}_N\right]_{p,p+1}$ with the phase calibration errors. In addition to these calibration errors, there are phase fluctuations between these elements caused by the finite sample support T. Therefore, by increasing the sample support T we can improve the "calibration" phase estimation accuracy. Indeed, the data in TABLE IV. are exactly the same as the data in TABLE III. despite using the estimated $\arg(\hat{t}_1)$ instead of the true one. This factor fully supports the provided interpretation of the described phenomenon.

TABLE IV.

"Invariant" Alg with $\arg(\hat{t}_1)$ (106). Phase errors: Sqrt 2nd moment (deg). Linear shift removed.		**N=17**		**N=100**	
		φ_{max}		φ_{max}	
		5^o	180^o	5^o	180^o
T	**100**	9.5	9.5	29.9	29.9
	300	5.5	5.5	16.9	16.9
	3E3	1.8	1.8	5.3	5.3
	3E4	0.5	0.5	1.7	1.7

Note finally that the existing complex Wishart distribution of the sample covariance matrix provides an exhaustive analytical description of these finite sample volume-related phase fluctuations that limit the accuracy of the estimation method (106). Note also that the error in $\arg(\hat{t}_1)$ leads to an additional linear phase "rump" (linear progression) along the aperture, although it's insignificant in some applications. For this reason, we conducted beamforming for the vector $\exp i\widehat{\Phi}_{N-1}$, and estimated the direction of the main peak, which exists for $\arg(\hat{t}_1) \neq \arg(t_1)$. Not surprisingly, after removal of the phase progression associated with the main peak position from $\widehat{\Phi}_{N-1}$, the estimation accuracy remained the same irrespective of the accuracy of $\arg(\hat{t}_1)$.

To conclude this algorithm, we analyzed the performance of our ad-hoc algorithm (64)-(66) proposed in [16] for the a priori known covariance matrix case. Simulations conducted for the same scenarios as the ML algorithm (55) revealed significant accuracy losses compared with the optimal algorithm (55). As follows from TABLE V. , these losses reach 82.7° for N = 17, T = 100, and get reduced slightly for the larger sample volume $T = 3{\cdot}10^4$. Recall that the described above "invariant" and "ad-hoc" estimation routines do not directly depend on the d/λ (linear shift) ratio in the ULA.

Let us now analyze the performance of the technique proposed in [6] in Sec IV for the over-sampled antenna regime.

TABLE V.

Ad-hoc Alg (66). Phase errors: Sqrt 2nd moment (deg). Linear shift removed.		**N=17**		**N=100**	
		φ_{max}		φ_{max}	
		5^o	180^o	5^o	180^o
T	**100**	82.7	82.7	103.7	103.7
	300	47.3	47.3	102.6	102.6
	3E3	9.7	9.7	19.8	19.8
	3E4	3.1	3.1	5.5	5.5

For a fair comparison, we consider the same covariance matrices as (28)-(30) and the same d/λ values for the linear phase progression in $\mathrm{diag}(\theta_0)$ (29). First let us prove in our prediction for the symmetric real-valued Toeplitz matrix $\mathbf{T}_N$ that the optimum (real-valued) solution coincides with the initial solution for $\boldsymbol{\psi}_N = 0^{\circ}$. Indeed, for the gradient optimization technique there is no way to move from $\boldsymbol{\psi}_n =$

$0, n = 1, \dots, N-1$ to $\boldsymbol{\psi}_n = (0, \pi)$, which requires a different optimization technique. For a real-valued covariance matrix shifted by $\theta = 20^o$, the optimum solution is presented in Fig. 48.

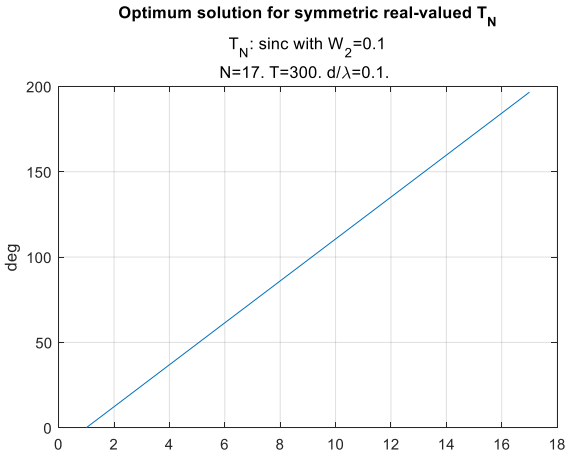

Fig. 48. Optimum solution for symmetric real-valued $\boldsymbol{T}_N$. $W_2 = 0.1$. $d/\lambda = 0.1$.

With an obvious linear trend that "returns" the spatial spectrum to its symmetric form with respect to $\theta = 0^o$ position, one can clearly see the symmetric non-linear component that, together with the linear shift, reduces the "invisible" power from the initial value 2.3 to 0.75. This example proves that our prediction of the optimum phase distribution in the absence of "calibration" phase errors is not just the linear progression for non-symmetric spatial spectra of the input signal.

Let us now prove our expectation that for the finite training sample support, the optimum solution for the case with the phase "calibration" errors present $\widehat{\boldsymbol{\phi}}_N$ is practically the sum of the "calibration" phase errors $\mathbf{E}_{\text{err}}$ and the optimum phase distribution for the no "calibration" phase errors case $\boldsymbol{\phi}_N^{(0)}$:

$$\boldsymbol{\Delta}_N = \widehat{\boldsymbol{\phi}}_N - \left(\boldsymbol{\phi}_N^{(0)} + \mathbf{E}_{\text{err}}\right) \to 0\,. \tag{107}$$

The simulation results illustrated below have been produced for the spatial spectrum shifted by $\theta = 20^o$ for the symmetric covariance matrix

$$\mathbf{T}_N = \text{sinc}\, W_2 + \sigma_l^2 \mathbf{I}_N\,, \quad W_2 = 0.1 \tag{108}$$

of the N = 17-element ULA. The sample volume is T = 300 and the number of independent trials is K = 100. For each trial we first ran the "no calibration errors" case followed by the case with "calibration" errors and then calculated $\boldsymbol{\Delta}_N$ in (107). Simulations have been conducted for $d/\lambda = 0.1, 0.2, 0.3, \text{and } 0.4$. In Fig. 49 we introduce the histogram of RMSE values for the vector $\boldsymbol{\Delta}_N$ for $d/\lambda = 0.1$.

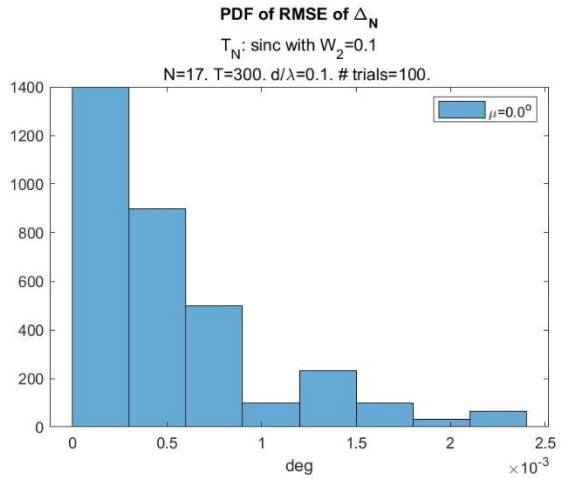

Fig. 49. PDF of RMSE of $\boldsymbol{\Delta}_N$. $\boldsymbol{T}_N$: $W_2 = 0.1$. $d/\lambda = 0.1$.

The RMSE of $\boldsymbol{\Delta}_N$ never exceeds $3 \cdot 10^{-3}$ in all 100 trials. The gain in invisible power (for the "no calibration errors" case) is illustrated in Fig. 50.

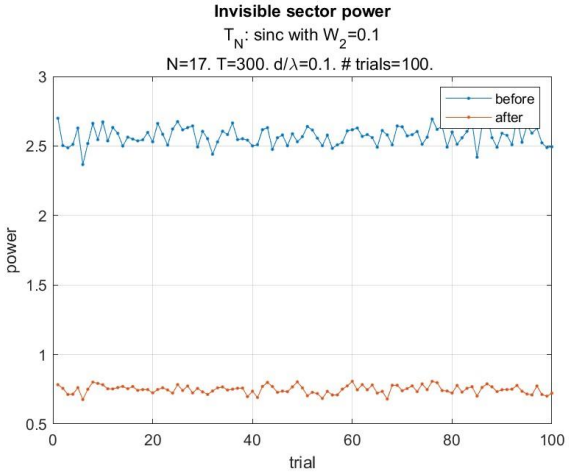

Fig. 50. Invisible sector power, before and after optimization. $\boldsymbol{T}_N$: $W_2 = 0.1$. $d/\lambda = 0.1$.

One can see that even for the "no phase errors" case, the optimum phase distribution reduces the invisible power by 6.53 dB. Finally in Fig. 51 we introduce all 100 optimum phase solutions derived for the "no phase errors" case. One can see that for this small $d/\lambda = 0.1$ the optimum phase distribution is practically a linear progression that "returns" the spatial spectrum to its symmetric (w.r.t. $\theta = 0^o$) position.

For $d/\lambda = 0.2$ the behavior of the optimum solution (for the "no phase errors" case) is more complicated (Fig. 52-Fig. 54).

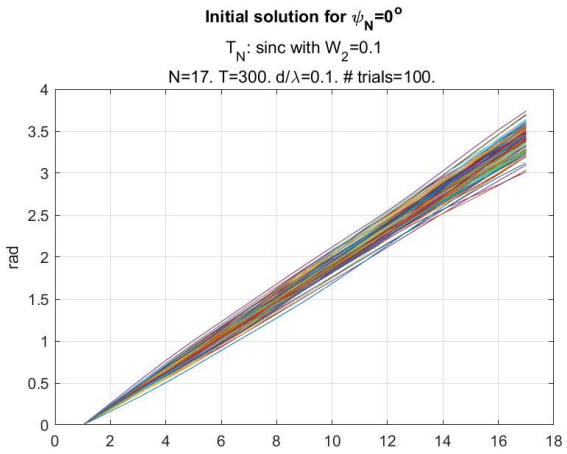

Fig. 51. Initial solution for $\psi_N = 0^o$ for 100 trials, where ψ_N is the "calibration" phase errors. $\boldsymbol{T}_N$: $W_2 = 0.1$. $d/\lambda = 0.1$.

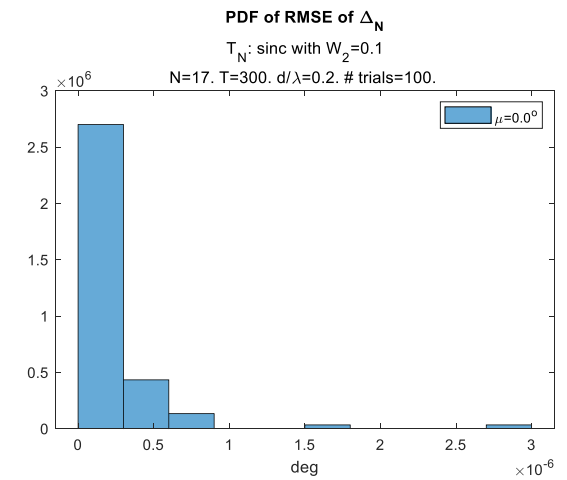

Fig. 52. PDF of RMSE of $\boldsymbol{\Delta}_N$. $\boldsymbol{T}_N$: $W_2 = 0.1$. $d/\lambda = 0.2$.

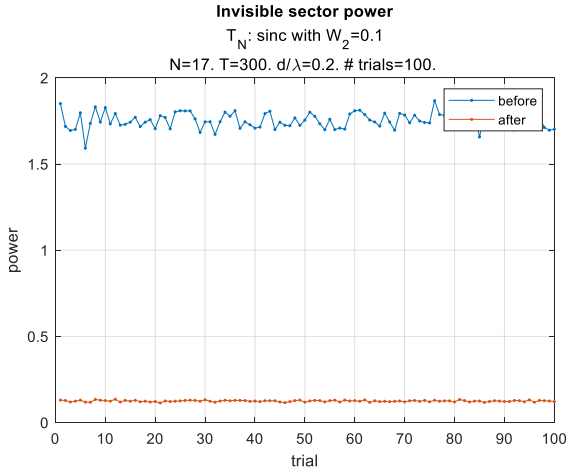

Fig. 53. Invisible sector power, before and after optimization. $\boldsymbol{T}_N$: $W_2 = 0.1$. $d/\lambda = 0.2$.

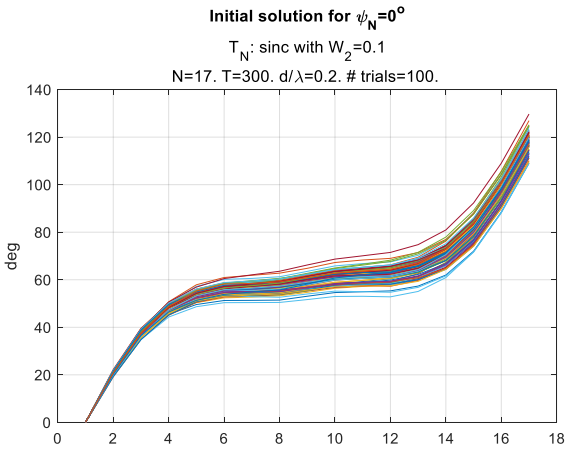

Fig. 54. Initial solution for $\psi_N = 0^o$ for 100 trials, where ψ_N is the "calibration" phase errors. $\boldsymbol{T}_N$: $W_2 = 0.1$. $d/\lambda = 0.2$.

First the RMSE of the vector $\boldsymbol{\Delta}_N$ does not exceed $3 \cdot 10^{-6}$, the gain in the suppressed power reaches ~20 dB ("no phase errors" case), and the optimum phase solution, being quite different from just the linear progression, closely follows the optimum deterministic ($T \to \infty$) solution (Fig. 55).

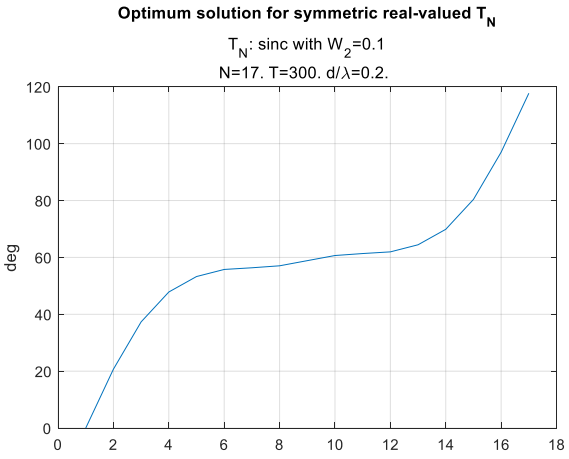

Fig. 55. Optimum solution for symmetric real-valued $\boldsymbol{T}_N$. $\boldsymbol{T}_N$: $W_2 = 0.1$. $d/\lambda = 0.2$.

For $d/\lambda = 0.3$ we observe the same 20 dB gain in "invisible" power as per $d/\lambda = 0.2$ (Fig. 57), with a more complicated optimum solution behavior (for the "no phase errors" case) (Fig. 58). Once again, in all 100 trials the optimum solutions closely follow the limit ($T \to \infty$) solution (Fig. 59).

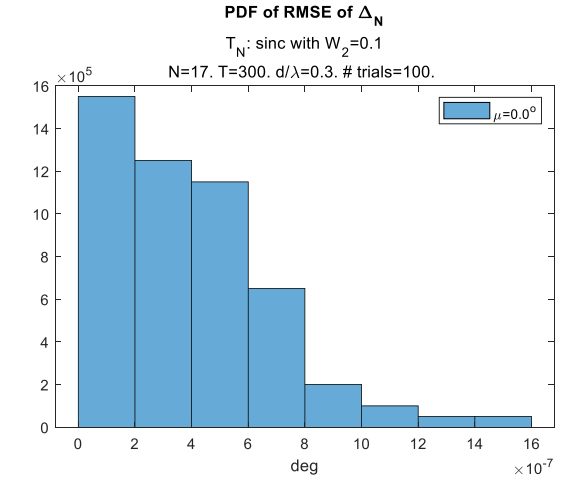

Fig. 56. PDF of RMSE of $\boldsymbol{\Delta}_N$. $\boldsymbol{T}_N$: $W_2 = 0.1$. $d/\lambda = 0.3$.

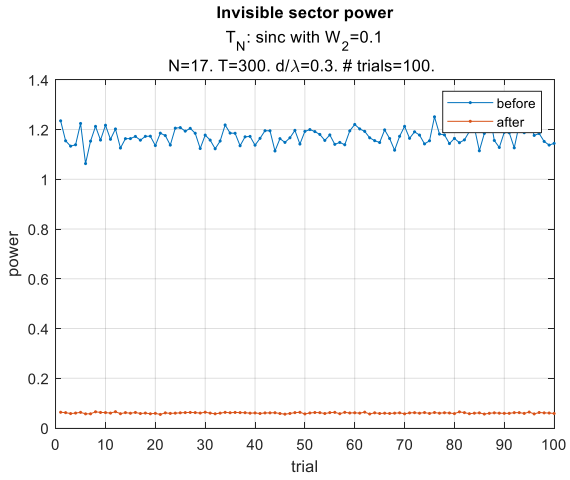

Fig. 57. Invisible sector power, before and after optimization. $\boldsymbol{T}_N$: $W_2 = 0.1$. $d/\lambda = 0.3$.

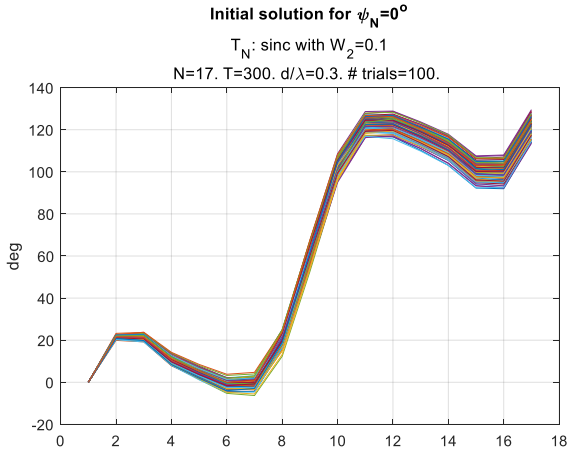

Fig. 58. Initial solution for $\psi_N = 0^o$ for 100 trials, where ψ_N is the "calibration" phase errors. $\boldsymbol{T}_N$: W_2. $d/\lambda = 0.3$.

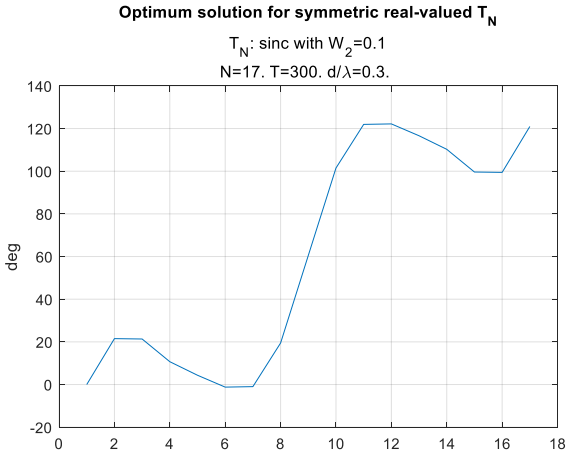

Fig. 59. Optimum solution for symmetric real-valued $\boldsymbol{T}_N$. $\boldsymbol{T}_N$: $W_2 = 0.1$. $d/\lambda = 0.3$.

For $d/\lambda = 0.4$, we observe quite different results over the 100 trials. Indeed, the RMSE error $\boldsymbol{\Delta}_N$ is significantly larger for this case. While most of the RMSE values are below 20°, in a few trials it reaches 100° (!). Correspondingly the "imaginary" power spectrum for the solutions with large $\boldsymbol{\Delta}_N$ is almost 10 times stronger than for the best solutions. The phase distribution for the "no phase errors" case is similar to the optimum for the $T \to \infty$ distribution, only for the solution with the best "invisible" power mitigation. Solutions that demonstrate a different behavior deliver much worse invisible power mitigation.

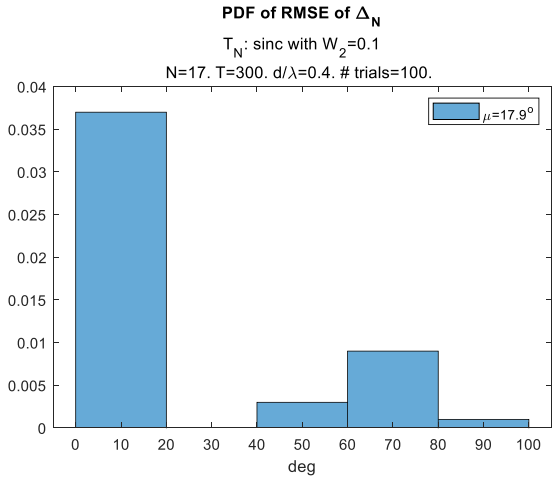

Fig. 60. PDF of RMSE of $\boldsymbol{\Delta}_N$. $\boldsymbol{T}_N$: $W_2 = 0.1$. $d/\lambda = 0.4$.

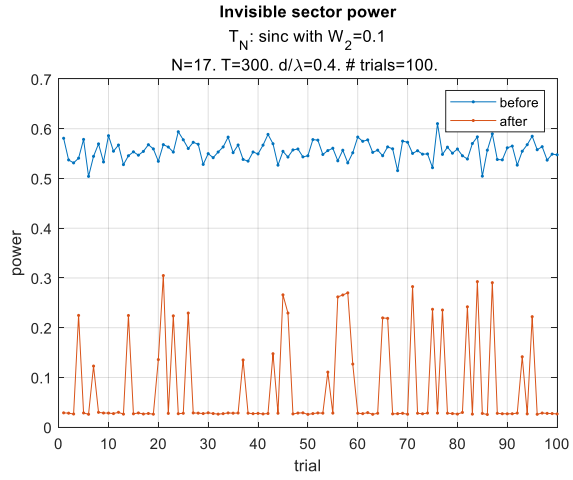

Fig. 61. Invisible sector power, before and after optimization. $\boldsymbol{T}_N$: $W_2 = 0.1$. $d/\lambda = 0.4$.

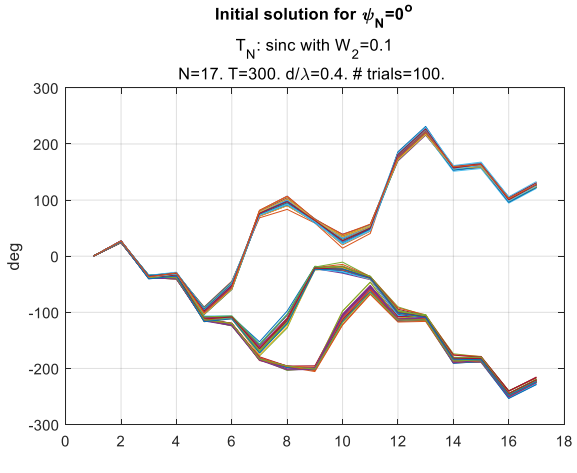

Fig. 62. Initial solution for $\psi_N = 0^o$ for 100 trials, where ψ_N is the "calibration" phase errors. $\boldsymbol{T}_N$: $W_2 = 0.1$. $d/\lambda = 0.4$.

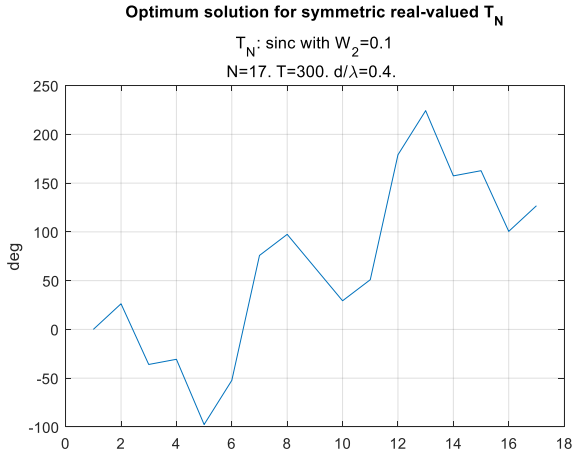

Fig. 63. Optimum solution for symmetric real-valued $\boldsymbol{T}_N$. $\boldsymbol{T}_N$: $W_2 = 0.1$. $d/\lambda = 0.4$.

Let us now analyze the results of the power distribution for the sinc functions shifted with respect to each other by $\theta = 20^{\mathrm{o}}$ for $W_1 = 0.2$ and $W_2 = 0.1$. For $d/\lambda = 0.1$ the RMSE of the "mismatch" vector $\boldsymbol{\Delta}_N$ (Fig. 64) is concentrated around 0.01^{o} but spreads up to 0.04^{o} over 100 conducted trials.

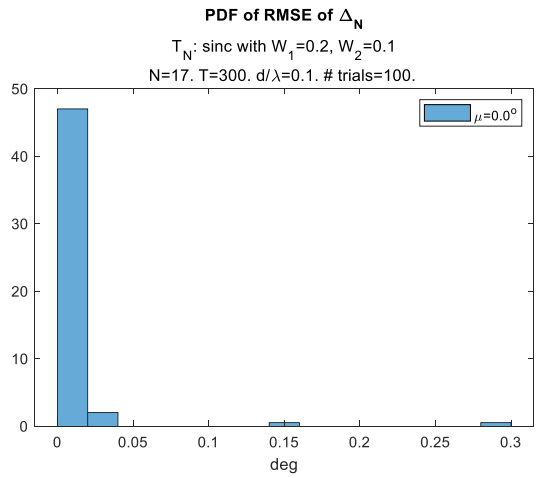

Fig. 64. PDF of RMSE of $\boldsymbol{\Delta}_N$. $\boldsymbol{T}_N$: $W_1 = 0.2, W_2 = 0.1$. $d/\lambda = 0.1$.

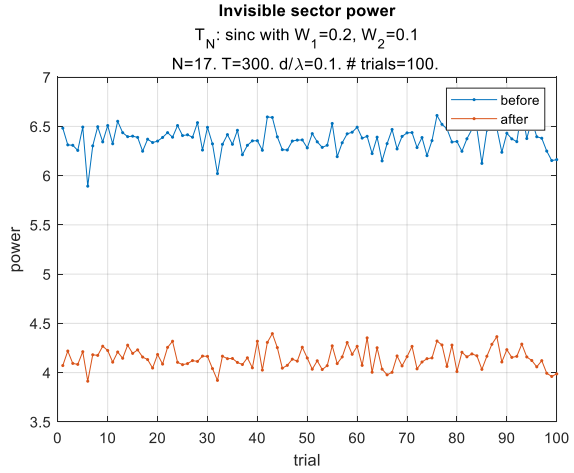

Fig. 65. Invisible sector power, before and after optimization. $\boldsymbol{T}_N$: $W_1 = 0.2, W_2 = 0.1$. $d/\lambda = 0.1$.

The "invisible" power is reduced on average by 6 dB only. While the optimized "no phase errors" case phase distribution is similar to the optimal $T \to \infty$ solution (Fig. 67), one can observe a noticeable difference in the derivative of this mostly linear progression over the 100 trials.

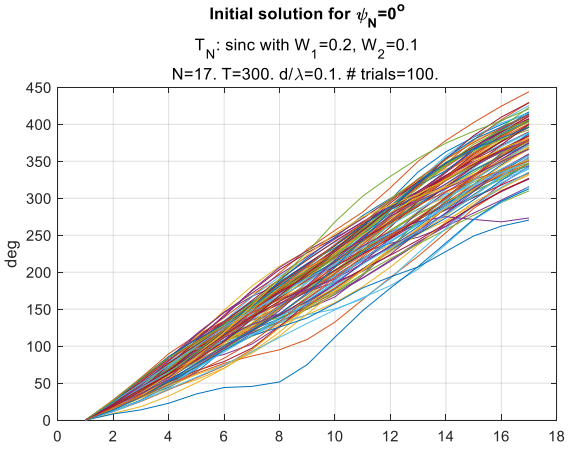

Fig. 66. Initial solution for $\psi_N = 0^o$ for 100 trials, where ψ_N is the "calibration" phase errors. $\boldsymbol{T}_N = W_1 = 0.2, W_2 = 0.1. d/\lambda = 0.1$.

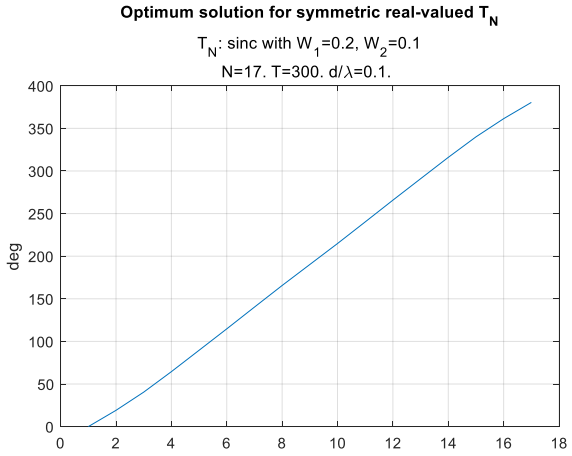

Fig. 67. Optimum solution for symmetric real-valued $\boldsymbol{T}_N = W_1 = 0.2, W_2 = 0.1. d/\lambda = 0.1$.

For $d/\lambda = 0.2$ the solutions are much more concentrated around the linear progression observed in the $T \to \infty$ case (Fig. 71), though the power gains over all 100 trials (Fig. 69) remain the same, around 5-6 dB. The most significant distinction with respect to the $d/\lambda = 0.1$ case is the very small RMSE of the vector $\boldsymbol{\Delta}_N$, which remains below $3{\cdot}10^{-7}$ º.

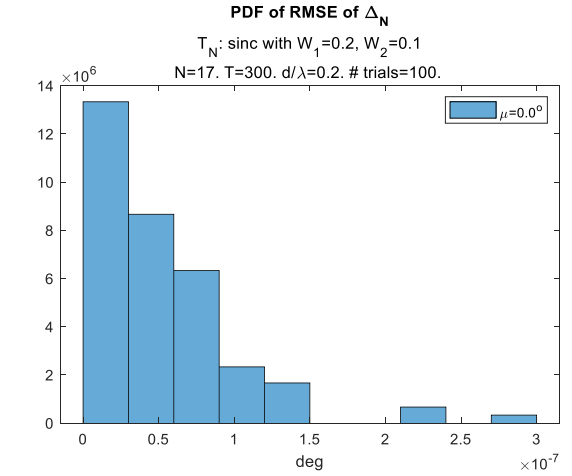

Fig. 68. PDF of RMSE of $\boldsymbol{\Delta}_N$. $\boldsymbol{T}_N$: $W_1 = 0.2, W_2 = 0.1$. $d/\lambda = 0.2$.

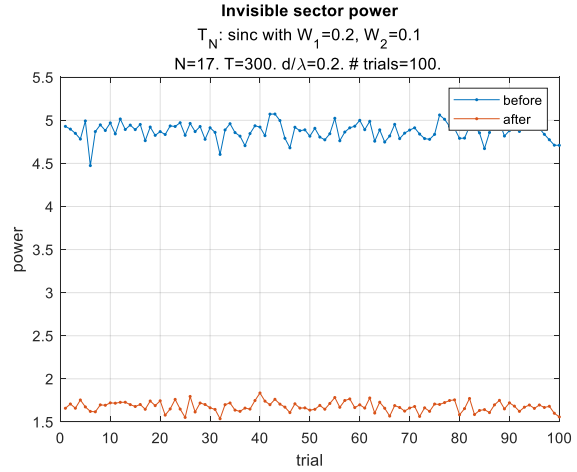

Fig. 69. Invisible sector power, before and after optimization. $\boldsymbol{T}_N$: $W_1 = 0.2, W_2 = 0.1$. $d/\lambda = 0.2$.

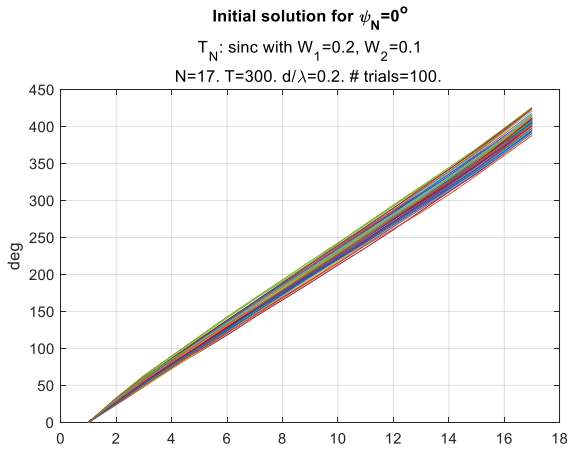

Fig. 70. Initial solution for $\psi_N = 0^o$ for 100 trials, where ψ_N is the "calibration" phase errors. $\boldsymbol{T}_N = W_1 = 0.2, W_2 = 0.1. d/\lambda = 0.2$.

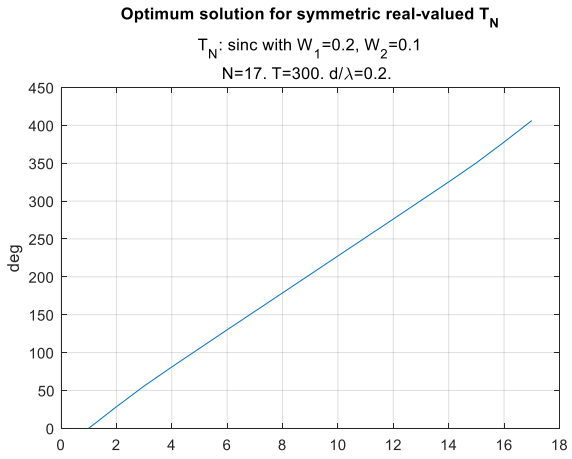

Fig. 71. Optimum solution for symmetric real-valued $\boldsymbol{T}_N = W_1 = 0.2, W_2 = 0.1. d/\lambda = 0.2$.

For $d/\lambda = 0.3$ we observe a more significant "invisible" power mitigation (~8 dB) and a noticeable departure of the optimum phase vector from the purely linear trend observed for the smaller d/λ.

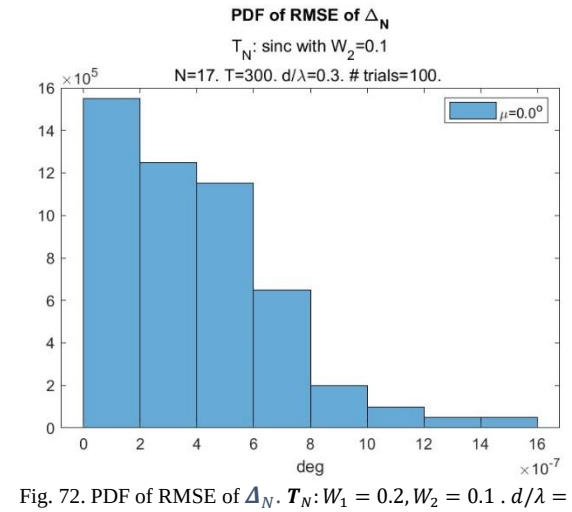

Fig. 72. PDF of RMSE of $\boldsymbol{\Delta}_N$. $\boldsymbol{T}_N$: $W_1 = 0.2, W_2 = 0.1$. $d/\lambda = 0.3$.

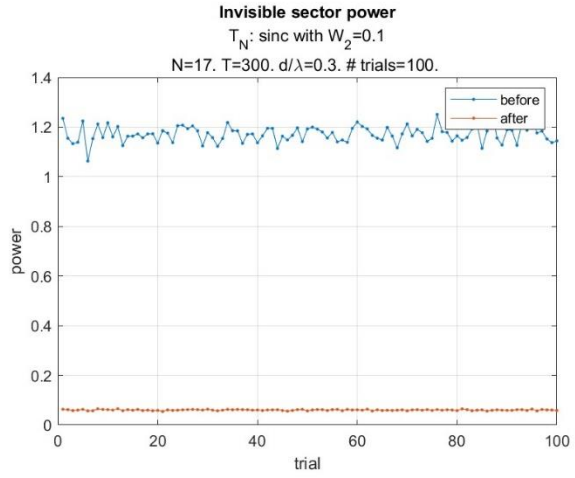

Fig. 73. Invisible sector power, before and after optimization. $\boldsymbol{T}_N$: $W_1 = 0.2, W_2 = 0.1.\ d/\lambda = 0.3.$

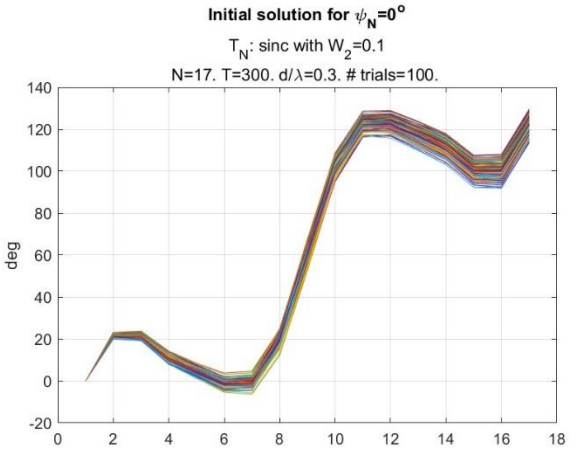

Fig. 74. Initial solution for $\psi_N = 0^o$ for 100 trials, where ψ_N is the "calibration" phase errors. $\boldsymbol{T}_N = W_1 = 0.2, W_2 = 0.1.\ d/\lambda = 0.3.$

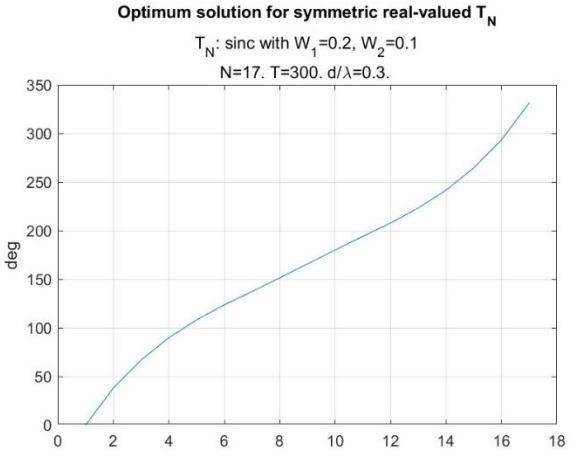

Fig. 75. Optimum solution for symmetric real-valued $\boldsymbol{T}_N = W_1 = 0.2, W_2 = 0.1.\ d/\lambda = 0.3.$

For $d/\lambda = 0.4$ the RMSE value for the vector $\boldsymbol{\Delta}_N$ once again degrades to $> 5{\cdot}10^{-3}$ °, providing ~26 dB "invisible" power mitigation (Fig. 77). All 100 trials demonstrate an insignificant departure from the ultimate $T \to \infty$ solution (Fig. 79).

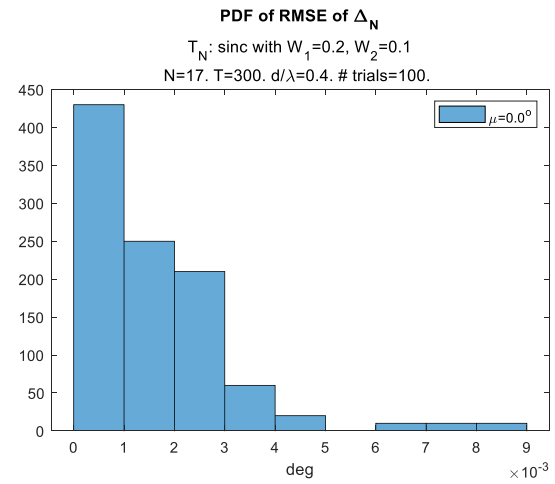

Fig. 76. PDF of RMSE of $\boldsymbol{\Delta}_N$. $\boldsymbol{T}_N$: $W_1 = 0.2, W_2 = 0.1\ .\ d/\lambda = 0.4.$

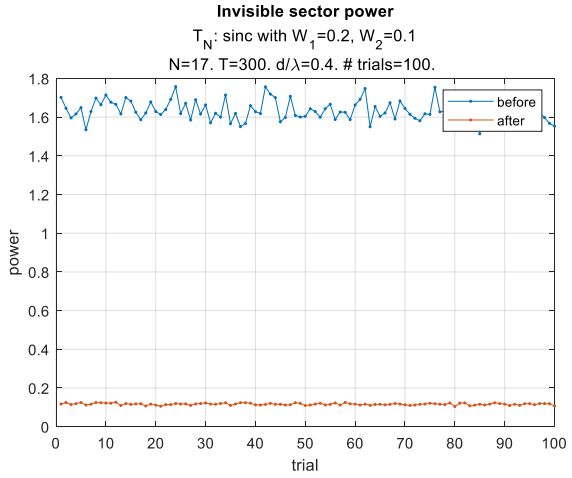

Fig. 77. Invisible sector power, before and after optimization. $\boldsymbol{T}_N$: $W_1 = 0.2, W_2 = 0.1.\ d/\lambda = 0.4.$

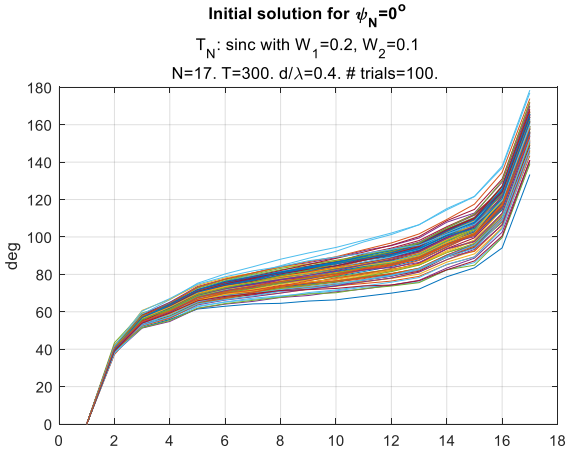

Fig. 78. Initial solution for $\psi_N = 0^o$ for 100 trials, where ψ_N is the "calibration" phase errors. $\boldsymbol{T}_N = W_1 = 0.2, W_2 = 0.1.\ d/\lambda = 0.4.$

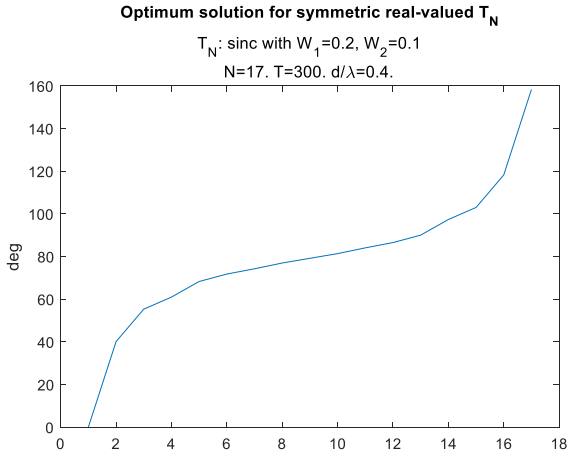

Fig. 79. Optimum solution for symmetric real-valued $\boldsymbol{T}_N = W_1 = 0.2, W_2 = 0.1. d/\lambda = 0.4$.

Most importantly these deviations do not lead to the optimized "invisible" output power variations. Therefore, the conducted trials fully support our expectations regarding the structure of the optimum phase solution. In all cases, the optimum solution, up to a small random error associated with the finite sample support, represents a sum of the phase "calibration" errors and phase distribution that minimizes the "invisible" power in a fully calibrated linear array. For the relatively small $d/\lambda < 0.2 - 0.25$ values, this second component is mainly a linear phase progression that finds the best (central) position of the spatial spectrum within the visible arc. This linear progression may be treated with bias removal, similar to the other phase "calibration" errors removal techniques. As previously mentioned, this bias in a properly calibrated ULA may be mitigated using HF radio stars with well-known coordinates. For $d/\lambda = 0.1$ and a small considered antenna array (N = 17), the optimum phase distribution for the "no collaboration errors" case substantially differs from the linear phase progression.

Since the reactive ("invisible") power reduction is useful for the operational solutions, these "combined" optimal phase distributions may be used for antenna calibration. In all these cases where such an approach is not applicable, one has to apply techniques for the joint "calibration" phase errors estimation, coupled with estimation of the Toeplitz spatial covariance matrix. These techniques are introduced in Part II of this series [19].

VI. Conclusions and Recommendations

In this paper we analyzed the benchmark efficiency and performance of the "blind" uniform array calibration techniques for the multi-element uniform linear arrays in applications for modern HF OTH radars. The attention to the "blind" antenna calibration techniques is stimulated by the broad introduction of the Direct Digital Receivers that provide simultaneous access to a large number of frequency channels within the entire HF band. Array calibration of a radar operating in passive mode requires different calibration techniques than the ones traditionally used in active radar channels, and the "blind" techniques that rely upon high accuracy of the array construction but do not require special test signals, match this application almost perfectly. Yet, analysis of the "benchmark" efficiency of the "blind" phase calibration errors estimation demonstrated the so called "strong" convergence requirements, whereby for the phase "calibration" errors estimation with the required high accuracy, an asymptotically large i.i.d. training sample volume is required. This property is demonstrated by the re-derived CRB for the "benchmark" scenario and by the results of the Monte-Carlo simulations of the ML-optimal estimation algorithm. Analysis of the few ad-hoc estimation algorithms that rely upon the Toeplitz structure of the spatial covariance matrix in the fully calibrated ULA but do not require this matrix estimate, demonstrated essential performance degradation with respect to the "benchmark" scenario. Specifics of the HF OTHR operations in the oversampled regime ($d/\lambda < 0.5$) allowed us to propose in [6] a novel calibration technique associated with the reduction of the received signal power in the so-called "invisible" antenna region. In the conference paper [6] where we proposed this technique, we demonstrated high efficiency of this approach for beamsteering orthogonal to the array line. In this paper this approach is analyzed in more detail. Specifically, we demonstrated that when the array beamsteering direction is not orthogonal, the "invisible" power mitigation optimum phase-only solution is non-trivial even for the properly calibrated antenna.

We demonstrated that on top of the linear phase progression that "returns" beams orthogonally to the array position, the significant non-linear components in the optimum phase distribution over the ULA's aperture are present, especially for arrays with close to $d/\lambda = 0.5$ inter-element spacing.

We demonstrated that for large training samples required for high array calibration accuracy, the optimum phase distribution in the presence of phase calibration errors with very high accuracy is the sum of the compensated "calibration" phase errors and phase distribution, optimum for the ideally calibrated array. In a number of applications, the reduction of reactivity of the oversampled array is a positive feature that can be practically used. If the truly Toeplitz nature of the spatial covariance matrix needs to be retained, it could be done by the Gohberg-Semencul transformation of the non-Toeplitz (after phase errors correction) spatial covariance matrix. Since this approach involves a spatial covariance matrix transformation, it is analyzed in detail in our next paper [19]

References

[1] D.A. Holdsworth, K. Mulder, M.D.E. Turley, "Jindalee operational radar network: new growth from old roots", *2022 IEEE Radar Conference*, (RadarConf 22), ieeexplore.ieee.org

[2] S.J. Anderson, B.D. Bates, M.A. Tyler, "HF surface-wave radar and its role in littoral warfare", *Journal of Battlefield Technology*, vol. 1, no. 3, Nov. 1999, pp. 23-28.

[3] "Advanced digital receivers", BAE Systems, https://www.baesystesms.com

[4] A. Paulraj, T. Kailath, "Direction of arrival estimation by eigenstructure methods with unknown sensor gain and phase", *Proc IEEE ICASSP '85*, Tampa FL, pp. 640-643, 1985

[5] A. Weiss, A Yeredor, "Asymptotically optimal blind calibration of uniform linear sensor arrays for narrowband gaussian signals", *IEEE Trans on Signal Processing*, vol 68, 2020, pp. 5323-5333.

[6] Y.I. Abramovich, G. San-Antonio, "Oversampled receive array calibration", *23rd European Signal Processing Conference (EUSIPCO)*, pp. 529-533.

[7] R.J. Muirhead, “Aspects of multivariate statistical theory”, John Willey & sons, inc, 1982
[8] Y.I. Abramovich, N.K. Spencer, A.Y. Gorokhov, “Bounds on maximum likelihood ratio – part I: applicataion to antenna array detection-estimation with perfect waveform coherence”, *IEEE on Signal Processing*, vol. 52, no. 6, July 2004, pp. 1524-1536.
[9] J. Vinogradova, R. Couillet, W. Hachem, “Estimation of toeplitz covariance matrix in large dimensional regime with application to source detection”, arXiv: 1403.1243 v.1 [CSIT], 5 March, 2014.
[10] K.C. Indukumar, V.U. Reddy, “A note on redundancy averaging”, *IEEE Trans on Signal Processing*, vol 40, no. 2, Feb 1992, pp. 466-469.
[11] Y.I. Abramovich, D.Z. Arov, V.G. Kachur, "Adaptive cancellation filters for stationary interference with a toeplitz correlation matrix”, in *Sov. J. Comm. Tech. Elect.*, vol. 33, No. 4, 1988, pp 54-61
[12] J. Chun, T. Kailath, "A constructive proof of the gohberg-semencul formula", *Linear Algebra and its Applications*, 1989, 121, pp. 475-489
[13] Y.I. Abramovich, T. Pongsiri, “Toeplitz inverse eigenvalue problem: application to the uniform linear array calibration”, arXiv:2305.13394, https://doi.org/10.48550/arXiv.2305.13394
[14] B.T. Polyak, Ya.Z. Tsypkin, “Criterion algorithms of stochastic optimization”, Automation and Remote Control (Translation from Russian), vol 46, No 6, Part 2, June 1984, pp. 766-771
[15] X. Mestre, “Improved estimation of eigenvalues and eigenvectors of covariance matrices using their sample estimates”, *IEEE Trans. on Information Theory*, vol. 54, no. 11, Nov. 2008, pp. 5113-5129.
[16] D.R. Fuhrmann," Estimation of sensor gain and phase”, *IEEE Transactions on Signal Processing*, vol. 42, No. 1, 1994, pp. 77-87
[17] D. Zwillinger, “Table of integrals, series and products”, Eighth Edition, USA: Elsevier, 2014.
[18] R.C. Voges, J.K. Butler, “Phase optimization of antenna arrays gain with constrained amplitude excitation”, *IEEE Trans on Antenna and Propagation*, vol AP-20, no. 4, July 1972, pp. 432-436.
[19] Y.I. Abramovich, V.I.Abramovich, T. Pongsiri, “’Blind’ calibration and Toeplitz covariance matrix estimation in uniform linear arrays. part II joint ‘blind’ calibration and Toeplitz spatial covariance matrix estimation”, to be published